Science of the Total Environment 438 (2012) 372–388

Contents lists available at SciVerse ScienceDirect

Science of the Total Environment

journal homepage: www.elsevier.com/locate/scitotenv

Micro- and nano-environments of C sequestration in soil: A multi-elemental STXM–NEXAFS assessment of black C and organomineral associations

Dawit Solomon [a,*], Johannes Lehmann [a], Jian Wang [b], James Kinyangi [a], Karen Heymann [a], Yingshen Lu [b], Sue Wirick [c], Chris Jacobsen [d]

[a] Cornell University, Ithaca, NY 14853, USA
[b] Canadian Light Source Inc., Saskatoon, Canada SK S7N 0X4
[c] National Synchrotron Light Source, Upton, NY 11973, USA
[d] Advanced Photon Source, Argonne, IL 60439, USA

HIGHLIGHTS

- STXM-NEXAFS identified terminal micro- and nano-organic C repository environments in undisturbed organomineral assemblage
- Produced multi-element images and fingerprint of physically entrapped particulate black C, non-black C and mineral matter
- Provided submicron-level multi-element insight about the most likely binding mechanisms in the organomineral interface
- Provided evidence for a "two-way" direct associative interaction between black C, non-black C and mineral matter
- Provided evidence for "three-way" indirect molecular-level linkage between black C, non-black C and mineral matter

ARTICLE INFO

Article history:
Received 2 February 2012
Received in revised form 23 August 2012
Accepted 24 August 2012
Available online xxxx

Keywords:
Biotic exclusion zone
C sequestration
Global C cycling
Organomineral interactions
Spatial inaccessibility
Soft X-ray spectromicroscopy

ABSTRACT

Black C is an essential component of the terrestrial C pool and its formation is often credited as a CO_2 sink by transferring the fast-cycling C from the atmosphere–biosphere system into slower cycling C in the geosphere. This study is the first multi-element K- (C, N, Ca, Fe, Al and Si) soft-X-ray STXM–NEXAFS investigation conducted at a submicron-scale spatial resolution specifically targeting black C and its interaction with the mineral and non-black C organic matter in the organomineral assemblage. The STXM–NEXAFS micrographs and spectra demonstrated that pyrogenic C was dominated by quinoide, aromatic, phenol, ketone, alcohol, carboxylic and hydroxylated- and ether-linked C species. There was also evidence for the presence of pyridinic, pyridonic, pyrrolic, amine and nitril N functionalities. The non-black C organic matter contained amino acids, amino sugars, nucleic acids and polysaccharides known to exhibit negatively charged carboxylic, phenolic, enolic, thiolate and phosphate functionalities highly reactive towards metal ions and black C. The metal-rich mineral matrix was composed of phyllosilicate clay minerals, Fe and Al hydroxypolycations, oxides, hydroxides and oxyhydroxide that can attract and bind organic biopolymers. STXM–NEXAFS provided evidence for interactive association between pyrogenic C, non-black C organic matter and the mineral oxide and oxyhydroxide communities in the organomineral interface. These intimate associations occurred through a "two-way" direct linkage between black C and the mineral or non-black C organic matter or via a "three-way" indirect association where non-black C organic matter could serve as a molecular cross-linking agent binding black C with the mineral matrix or vice versa where inorganic oxides, hydroxides and polycations could act as a bridge to bind black C with non-black C organic matter. The binding and sequestration of black C in the investigated micro- and nano-C repository environments seem to be the combined action of physical entrapment in seemingly terminal biotic exclusion zone through the action of metal oxides and organic matter induced microaggregation and through molecular-level association ranging from ligand exchange, polyvalent cation bridging to weak hydrophobic interactions including van der Waals and H-bonding.

1. Introduction

Soils, the complex biomaterials that promote growth of terrestrial organisms, are an integral compartment of the Earth's environment and the central organizer of ecosystem processes interacting constantly with the atmosphere, biosphere, and hydrosphere as a

* Corresponding author. Tel.: +1 607 255 1730; fax: +1 607 255 2644.
E-mail address: ds278@cornell.edu (D. Solomon).

0048-9697/$ – see front matter © 2012 Elsevier B.V. All rights reserved.
http://dx.doi.org/10.1016/j.scitotenv.2012.08.071

consequence of natural cycles and human activities (Huang, 2004). Global soils represent the largest reservoirs of terrestrial organic C pool (3300 Pg) in the biosphere, storing more C than is contained in all living plants (560 Pg) and the atmosphere (760 Pg) combined (Tarnocai et al., 2009). If this vast amount of C is destabilized through anthropogenic intervention and climate change, it can lead to accelerated emissions of greenhouse gases and could make a significant difference in the Earth's atmospheric composition. Despite its importance, however, the underlying biogeochemical mechanisms that control the long-term sequestration of soil C and the potential to further increase the current soil C storage capacity are not yet well understood and the full potential for C sequestration in the Earth's surface remains unknown (Trumbore, 2009).

The earliest investigations of soil C were documented in the 18th century (Achard, 1786) and the importance of the association between C and minerals in soil has been recognized more than one hundred years ago (Schloesing, 1902). It is, therefore, all the more astonishing that the precise geobiological mechanisms for the interaction between minerals and organic C in soils are still largely unknown.

Soil organic C is composed of a complex mixture of organic compounds released from living plant and microbial cells to complex plant, animal and microbial residues ranging in size and complexity from simple monomers to complex biopolymers (Baldock and Skjemstad, 2000). Its composition is also strongly influenced by fire, which can thermally modify the structural chemistry of the incoming biomass and detrital C resulting in the formation of a suite of refractory carbonaceous substances ranging from partially charred biomass to highly graphitized soot; collectively referred to as black C (Preston and Schmidt, 2006). Black C is one of the most ubiquitous materials in the environment, and it is often regarded as a chemically and biologically stable C pool that can persist in nature for a very long time. The formation of black C is credited as a CO_2 sink by transferring fast-cycling C from the atmosphere–biosphere system into much slower cycling C in the geosphere (Lehmann et al., 2005). Further impetus for black C research arises from the fact that it plays a key role in a wide range of chemical processes due to its amphipathic nature, and may serve as an effective sorbent for potentially hazardous organic compounds and other pollutants in soils (Loganathan et al., 2009). Literature evidence suggests that the mechanisms for stabilization of black C in soils appear to be the result of physicochemical processes involving (i) selective preservation of recalcitrant C molecules and extracellular neoformations, (ii) spatial inaccessibility of C due to localized "biotic exclusion" zones and (iii) inter-molecular interactions between C and minerals (Sollins et al., 1996; Lützow et al., 2006; Solomon et al., 2007). One of the major limiting factors to past investigations is that these processes operate at the micro-, nano- and atomistic-levels, well below the scale that most studies were able to observe C. Most of the information gathered so far about organomineral associations and interfacial chemical processes was obtained indirectly from approaches that involve batch experiments, gas-sorption analysis and oxidative or other wet-chemical techniques often performed under adverse experimental conditions that may not preserve natural conditions (Haumaier and Zech, 1995). Therefore, direct multi-element evidence for the precise mechanisms operating at micro-, nano- and atomistic scales will constitute a major breakthrough in soil science and could generate unparalleled opportunities to sequester C for climate change mitigation. With the advent of non-invasive synchrotron-based scanning transmission X-ray microscopy (STXM) and near-edge X-ray absorption fine structure (NEXAFS) spectroscopy techniques, it is now possible to circumvent the limitations of wet-chemical techniques and investigate not only the fine structures of C but also directly image organic C forms in nanometer spatial resolution (Kinyangi et al., 2006; Yoon et al., 2006; Lehmann et al., 2008). However, most of these investigations were conducted using beamlines optimized for C, but lacking energy fluxes to quantify the most abundant soil minerals restricting the information generated from these investigations mostly to C. STXM–NEXAFS has potential to access the K or L-edge of Ca, N, Fe, Al, Si and may lead to acquisition of spatially defined high-resolution geobiological information about submicron-C repository environments (Wan et al., 2007) and the molecular-level associations between organic C moieties, minerals and polyvalent metal ions, as well as other surficial and interactive features.

The objectives of the present investigation were (i) to identify, image and fingerprint the fine structures of black C present in intimate association with non-black C organic C and mineral matter in the micro- and nano-C repository environments of organomineral assemblage of a mineral soil and (ii) to conduct a submicron-level investigation of the compositional chemistry and interactive features of the various elements (N, Al, Si K-edge, and Ca and Fe $L_{2,3}$-edge) present in association with black C using novel non-destructive high-resolution STXM–NEXAFS spectromicroscopy.

2. Materials and methods

2.1. Study site description and sample background information

This study was conducted using soil samples collected from the Kakamega forest of western Kenya. The Kakamega forest is located at 00°14′19″N and 34°57′13″E. The natural vegetation is composed of tropical (*Aningeria altissima* A. Chev. and *Chrysophyllum albidum* G. Don) and montane (*Olea capensis* L. and *Croton megalocarpus* Hutchinson) forest tree species. The altitude of the area ranges from 1700 to 1800 m above sea level, with mean annual temperature of 19 °C and precipitation of 2080 mm. The soils of the area are well-drained, deep red to yellowish red, friable sandy clay loam to clay loam texture developed from undifferentiated basement system rocks and classified as Ferralo-Chromic Acrisols (FAO-UNESCO, 1997). The organic C content was 119 g kg^{-1} soil, total N was 11 g kg^{-1} soil, total S was 2.9 g kg^{-1} soil, with pH-KCl of 5.3. Detailed chemical properties can be found in Kinyangi et al. (2006).

2.2. Ultrathin section preparation

One gram of undisturbed soil was sieved to pass through a 250 μm sieve but trapped on a 150 μm sieve, and the free stable microaggregates were isolated. The microaggregates were sprinkled on a glass fiber filter (Whatman GF/A, 90 mm diameter), mounted onto a 1000 μm sieve surface, and fixed to a chimney funnel that transferred mist from a humidifier chamber filled with double deionized water. After 18 h of misting the microaggregates were considered to be water saturated. Excess droplets were drained off before shock-freezing the microaggregates. Lehmann et al. (2008) demonstrated that this procedure enables to observe the spatial arrangement of organic matter in organomineral assemblages without compromising the sample's spatial integrity. Approximately 150 μm diameter microaggregate subsample was selected and ultrathin section (400 nm) was produced at −55 °C using cryomicrotome. Glass knife attached to an ultramicrotome (Ultracut UTC, Leica Microsystems Inc., USA) was used for initial trimming and a diamond knife (Ultra 45 °C, Diatome Ltd., Switzerland) was employed for final cutting at 1.2 mm s^{-1}. The thin section was transferred to a silicon monoxide (SiO) impregnated copper grid (200 meshes, Ladd Research, USA) and stored in trays placed in wide mouth airtight Mason jar under argon environment. The Cu grid was mounted onto stainless steel sample stage plate for STXM–NEXAFS measurements. Details about the thin sectioning procedure are described by Kinyangi et al. (2006) and Lehmann et al. (2008).

2.3. Multi-element STXM and NEXAFS data acquisition and analysis

2.3.1. C K-edge spectromicroscopy

C NEXAFS was recorded at X1A1 beamline of the National Synchrotron Light Source (NSLS) using the STXM end station. The essential components of this beamline are a tunable undulator inserted in the 2.8 GeV electron storage ring generating a high-flux of photons at 10^7 spatially coherent photons s^{-1} in the soft X-ray region, a spherical grating monochromator with maximum spectra resolving power of 5000 lines mm^{-1}, a 160 μm Fresnel zone plate that can focus the beam to a 40 nm spot size for a maximum spatial resolution of up to 50 nm, and a proportional counter to detect the transmitted photons. The beamline slit width was set to 45/25/25 μm to provide an energy resolution of 0.1 eV. Both spectral and imaging resolutions of the beamline are described in depth elsewhere (Wirick et al., 2009). The monochromator was calibrated using CO_2 (290.7 eV). A stack data set was collected in transmission mode under He atmosphere by imaging in X and Y dimensions, then changing the monochromator by energy increments of 0.3 eV for the energy range from 280.0 to 282.5 eV (dwell time, DT, 1 ms), 0.1 eV from 282.6 to 292.0 eV (DT, 2 ms), 0.5 eV from 292.1 to 305.5 eV (DT, 3 ms) and 1.0 eV from 305.6 to 310.0 eV (DT, 4 ms). A smaller energy step (0.1 eV) was chosen at levels where core electrons of C can be excited (283.0–290.0 eV). After the entire microaggregate was scanned using a zone plate with 40 nm focused beam spot at 500 nm steps (described here as 500 nm spatial resolution), high-resolution scans were conducted at the various C repository zones or hotspots within the intact organomineral assemblage at a 50 nm spatial resolution (40 nm focused beam spot and at 50 nm steps here described as 50 nm spatial resolution) to probe the micro- and nano-C sequestration environments (Kinyangi et al., 2006; Lehmann et al., 2008; Wirick et al., 2009). Individual images recorded across all energy levels were built into a stack using the Stack Analyze 2.6.1 software (Jacobsen et al., 2000) and aligned in X and Y using cross-correlation (with 290.0 eV as a reference). For the spatial analyses, the stack data were orthogonalized and noise-filtered by principal component analysis as described in Lerotic et al. (2004) and Kinyangi et al. (2006). Cluster analysis was used to identify sample regions with similar spectral properties and to identify regions for which target spectra of organic C were defined in comparison with cluster spectra using PCA GUI 1.1.1 (Lerotic et al., 2004). The first 4 components and 12 clusters were used on the basis of the eigenvalues, eigenimages and eigenspectra calculated by the principal component analysis, without using the first principal component as described in Lerotic et al. (2004), Kinyangi et al. (2006) and Lehmann et al. (2008). Cluster analysis uses this subset of principal components to group similar spectra in the stack data set (Lerotic et al., 2004) and produce cluster maps. Stack image processing software and data analyses manuals can be accessed on the web at http://xray1.physics.sunysb.edu/data/software.php.

2.3.2. N, Al, Si K-edge, and Ca and Fe L-edge spectromicroscopy

The Ca, N, Fe, Al and Si NEXAFS measurements were performed using the STXM end station at the soft X-ray spectromicroscopy (SM) 10ID-1 beamline of the Canadian Light Source (CLS). The 10ID-1 beamline, inserted in a 2.9 GeV electron storage ring, consists of an APPLE II type Elliptically Polarizing Undulator (EPU), a Plane Grating Monochromator (PGM) optimized for photons from 100 to 2000 eV range. The STXM provides high quality imaging and spatially resolved spectroscopy with an on-sample flux of 10^8 photon s^{-1} focused by a Fresnel zone plate lens to a 30 nm focal spot sizes, with a 30 nm spatial resolution and spectral resolution power ($E/\Delta E$) that can reach up to ~10,000. Details about the STXM and the microscope can be found at Kaznatcheev et al. (2007) and http://www.lightsource.ca/experimental/pdf/SM_Beamline_Technical_Sheet.pdf.

Stack data sets for Ca, N, Fe, Al and Si were collected in transmission mode under He from the thin section used for C NEXAFS. Similar to C, image sequences were recorded in X and Y dimensions and then changing the monochromator in energy increments varying from 0.3 to 0.88 eV (depending on the element) first from the entire microaggregate using a zone plate with a focused spatial resolution of 500 nm and 50 nm scans were recorded at the same micro- and nano-regions identified using the center X and Y coordinates and ranges of the C NEXAFS images. The increasing energy flux and stack energy range parameters for high-resolution scans are provided as follows: (i) Ca L-edge 340.0–343.5 eV at 0.3 eV steps, 343.6–354.0 eV at 0.1 eV and 354.1–360.0 eV at 0.3 eV steps with 27/27 μm slit size and 1 ms DT; (ii) N K-edge 390.0–395.0 eV at 1 eV steps, 395.1–404.0 eV at 0.1 eV steps, 404.1–410.0 eV at 0.3 eV, and 411.1–430.0 at 1 eV steps with 27/27 μm slit size and 0.87 ms DT; (iii) Fe L-edge 700.0–704.0 eV at 0.5 eV steps, 704.1–713.0 at 0.2 eV steps, 713.1–718.0 at 1 eV steps, and 718.1–735.0 eV steps at 1.5 eV steps with 27/27 μm slit size and 0.87 ms DT; (iv) Al K-edge 1540.0–1558.0 eV at 1 eV steps, 1558.1–1575.0 at 0.2 eV steps, 1575.1–1585.0 at 1 eV steps, and 1585.1 1610.0 eV at 2 steps with 35/35 μm slit size and 0.87 ms DT; and (v) Si K-edge 1820.0–1830.0 eV at 1 eV steps, 1830.1–1860.4 at 0.2 eV steps, 1860.5–1880.5 at 0.5 eV steps, and 1880.6–1890.0 eV at 2 eV steps with 45/45 μm slit size and 0.95 ms DT. The stack data set was preprocessed using the stack fit and stack analyze routine of Analysis of X-ray Microscopy Images and Spectra (aXis2000), an Interactive Data Language (IDL) widget for processing X-ray spectra and images developed by Hitchcock (2008). Image processing and data analysis instructions to a format compatible with Stack Analyze (Jacobsen et al., 2000) and PCA GUI 1.1.1 (Lerotic et al., 2004) programs used for analyses of the C NEXAFS data can be accessed at http://unicorn.mcmaster.ca/aXis2000.html. Image sequences were aligned and converted to optical density (OD). Principal component and cluster analyses for each element were conducted as described in Section 2.3. The spectra were processed using WinXAS 3.1 (WinXAS software, Germany) as described in Solomon et al. (2009).

3. Results and discussion

3.1. C K-edge STXM–NEXAFS spectromicroscopy

The high-resolution C STXM–NEXAFS micrograph (Fig. 1a) calculated from -log (I/Io), where $I = \sum$ (280.0–282.9 eV) and $I_0 = \sum$ (290.0–310.0 eV) clearly identified the micro- and nano-scale variability in the chemical composition of organic C (light color) and mineral (darker color) matter (Fig. 1a). The spatially-resolved total organic C distribution map (Fig. 1a) recorded from the submicron-C repository environment of the investigated organomineral assemblage also showed a distinct and morphologically-discernable feature of physically entrapped particulate organic matter entity where C was occluded in a seemingly terminal repository environment. Differential analysis of this region further revealed that organic C fine structure composition of this carbonaceous entity appeared to be ostensibly pyrogenic in nature largely dominated by characteristic transitions associated with quinone (284.0–284.7 eV, Fig. 1b), aromatic (285.0–285.9 eV, Fig. 1c), phenolic and ketonic (286.0–286.9 eV, Fig. 1d) C functionalities (Brandes et al., 2004; Braun et al., 2007; Solomon et al., 2009). Although less abundant and mostly restricted to the outer surface of the particulate pyrogenic structure, transitions related to aliphatic and imidazole (287.0–287.9 eV, Fig. 1e), carboxylic/carbonyl and amide (288.0–288.9 eV, Fig. 1f), polysaccharide, amino sugar and alcohol species (289.0–289.9 eV, Fig. 1g) were also visible. These functionalities could be the results of organic matter sorption from non-black C sources or oxidation of organic C functionalities present on the surface of the investigated particulate pyrogenic particle. These suggestions are in agreement with the results of Lehmann et al. (2005), Liang et al. (2006) and

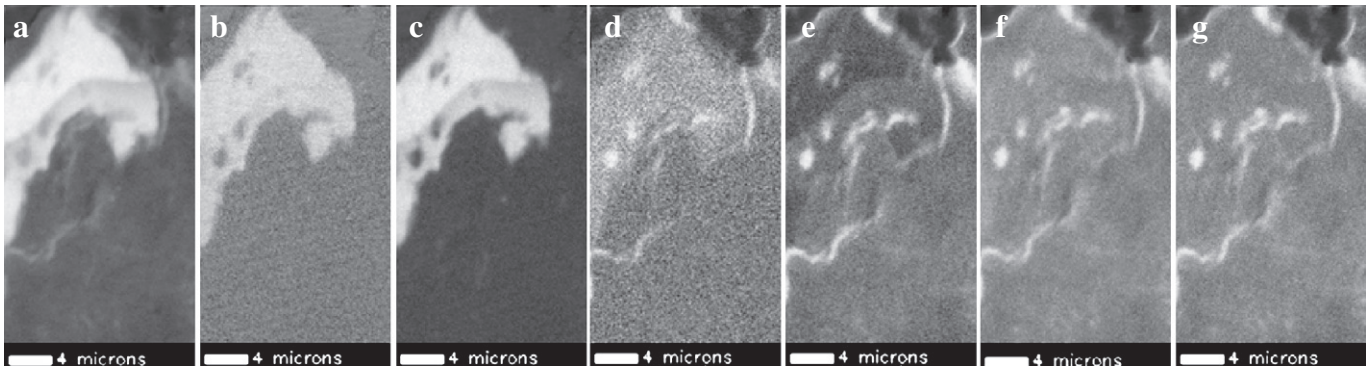

Fig. 1. C K-edge STXM–NEXAFS image showing spatial distribution of total organic C and mineral matter (a) in the organomineral assemblage and the various organic C forms associated with the particulate black C particle (b, quinones; c, aromatic-C; d, phenols and ketones; e, aliphatic and imidazole structures; f, carboxyl/carbonyl and amides; g, polysaccharides).

Solomon et al. (2007) where spectromicroscopy investigations provided a clear evidence for progressive surface oxidation and adsorption of organic C forms from non-pyrogenic C sources on the surface of black C particles isolated from mineral soils. Our results are also in line with the results of Brodowski et al. (2006) who found intact black C particles originating from vegetation fires and coal combustion physically occluded within the microaggregates with oxidized functionalities dominating the edge of these pyrogenic structures making them prone to interactions with soil minerals.

3.1.1. Nano-scale cluster analysis of C from the black C

The high-resolution C K-edge NEXAFS composition thickness map provided detailed features of the particulate black C particle (red color) and the nearby organomineral matrix (gray color) (Fig. 2a). The C K-edge cluster indices map (Fig. 2b) further exhibited various micro- and nano-regions in the inner (Fig. 2c), intermediate (Fig. 2d–e) and exterior (Fig. 2f) regions of the black C particle and the respective spectral features associated with these regions (Fig. 2m). According to Fig. 2m the spectra recorded from the black C particle exhibited good selectivity in the fine structure regions of the C k-edge spectra and revealed multiple absorption bands which correspond to characteristic C functionalities. These spectral signatures showed great similarity with the main C 1s–π* and 1s–3p/σ* transitions acquired from fresh charcoal, aged black C and anthracite coal (Lehmann et al., 2005; Liang et al., 2006; Yoon et al., 2006). Detailed analyses of the C 1s spectral signatures from the inner,

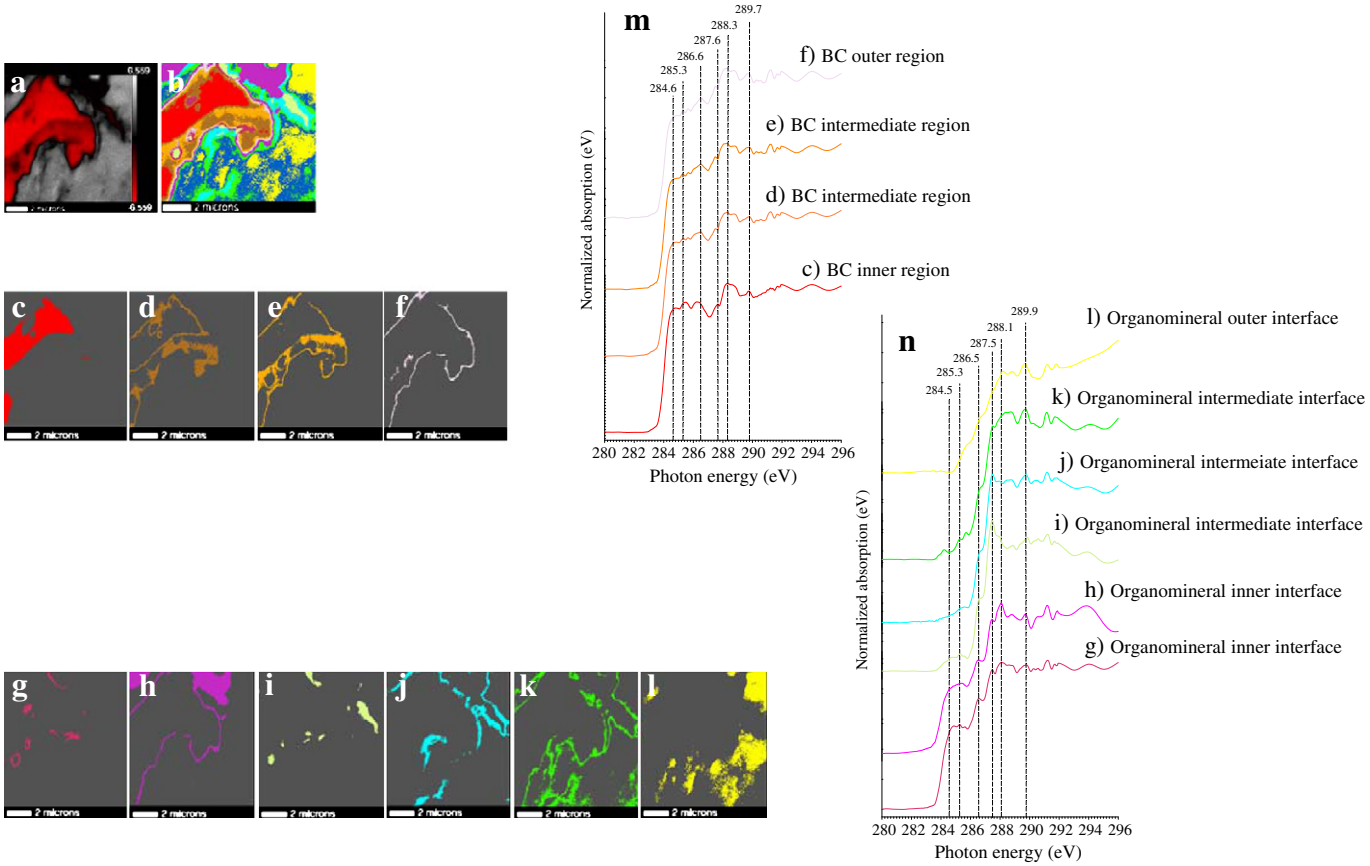

Fig. 2. High-resolution C K-edge composition thickness map (a), cluster index map (b) of the investigated submicron-C repository environment showing nano-scale distribution of C components and individual cluster images of the black C (c–f) and organomineral interface (g–l) regions and their respective C 1s NEXAFS spectra (m–n).

Table 1
Energy ranges, transitions and organic C structures from the particulate black C and the adjoining organomineral interface.

Energy ranges eV	Chemical group	Transitions	Structural examples
Particulate black C particle			
283.0–284.7	Quinone-C	C 1s–$\pi^*_{C=O}$	Aromatic quinones
	Diene-C	C 1–$\pi^*_{C=C}$	Fused ring structures of aromatic hydrocarbons and conjugated dienes
285.0–285.9	Aromatic-C	C 1s–$\pi^*_{C=C}$	Ring structures of polycyclic aromatic hydrocarbons
	Olefinic-C	C 1s–$\pi^*_{C=C}$	Unsaturated hydrocarbons and olefins
286.0–286.9	Phenolic-C	C 1s–$\pi^*_{C=C}$	Aromatic-C connected to O group (C–OH) in phenols
	Ketonic-C	C 1s–$\pi^*_{C=O}$	Carbonyl substituted aromatic structures of quinones, phenols and ketones
287.0–287.9	Aliphatic-C	C 1s–$\sigma^*/3p_{C-H}$	Aliphatic hydrocarbons
	Carbonyl-C	C 1s–$\pi^*_{C=O}$	Carbonyl functionalities from aromatic ketones
288.0–288.7	Carboxylic-C	C 1s–$\pi^*_{C=O}$	Carbonyl C in aromatic and unsaturated carboxylic acids
289.0–289.9	O-alkyl-C	C 1s–$\sigma^*/3p_{C-OH}$	Alcohols and hydroxylated- and ether-linked C species
	Carbonyl-C	C 1s–$\pi^*_{C=O}$	Aromatic alcohols and quinine structures
Organomineral interface			
283.0–284.7	Quinone-C	C 1s–$\pi^*_{C=O}$	Aromatic quinones
	Diene-C	C 1s–$\pi^*_{C=C}$	Fused ring structures of aromatic hydrocarbons and conjugated dienes
285.0–285.9	Aromatic-C	C 1s–$\pi^*_{C=C}$	Aromatic ring structures of hydrocarbons, amino acids and nucleobases
	Olefinic-C	C 1s–$\pi^*_{C=C}$	Unsaturated hydrocarbons and olefins
286.0–286.9	Phenolic-C	C 1s–$\pi^*_{C=C}$	Aromatic-C connected to O atom of hydroxyl group in phenols
	Ketonic-C	C 1s–$\pi^*_{C=O}$	Carbonyl substituted aromatic structures of quinones, phenols and ketones
	Imine-C	1s–$\pi^*_{C=N}$	Imine structures of aromatic amino acids and nucleobases
	Amide-C	C 1s–σ^*_{C-N}	Amide C in pyrrole side ring structures of amino acids and nucleobases
287.0–287.9	Aliphatic-C	C 1s–$\sigma^*/3p_{C-H}$	Aliphatic hydrocarbons
	Carbonyl-C	C 1s–$\pi^*_{C=O}$	Carbonyl functionalities from aromatic ketones
	Imine-C	C 1s–$\pi^*_{C=N}$	Imidazole ring structures of amino acids and nucleobases
288.0–288.7	Carboxylic-C	C 1s–$\pi^*_{C=O}$	Carbonyl C in carboxylic acids, aromatic alcohols and polysaccharide structures
	Aldehyde-C	C 1s–$\pi^*_{C=O}$	Aldehyde structures related to polysaccharides
	Carboxyamide-C	C 1s–$\pi^*_{C=O}$	Carboxyamide functionalities of amino sugars, amino acids and nucleobases
	Amide-C	C 1s–σ^*_{C-N}	Amide structures of amino acids and nucleobases
289.0–289.9	O-alkyl-C	C 1s–$\sigma^*/3p_{C-OH}$	O-alkyl-C of polysaccharides, amino sugars, nucleic acid, alcohols and ethers
	Carbonyl-C	C 1s–$\pi^*_{C=O}$	Aromatic alcohols, quinines and carbonyl structures of nucleobases
	Imide-C	C 1s–$\pi^*_{C=N}$	Amide structures of amino acids

intermediate and exterior regions of the black C (Fig. 2c–f) revealed broad resonances near 284.6 eV (Fig. 2m). Francis and Hitchcock (1992) and Haberstroh et al. (2006) indicated that such resonances are largely associated with lower π* energy states and usually considered as indication for the presence of C1s–$\pi^*_{C=O}$ transitions from quinones and quinoid structures of oxidized derivatives of polycyclic aromatic structures such as benzoquinone (Table 1). However, Solomon et al. (2009) observed a prominent resonance near 284.3 eV from fused aromatic ring structures of polycyclic aromatic hydrocarbons, while Kolczewski et al. (2006) reported broad symmetric peaks near this absorption band from cyclohexadiene and concluded that in pyrogenic structures such signatures could also be the results of 1s–π* excitations originating from double bonded C atoms of benzene and conjugated diene structures. The broad absorption bands near 285.3 eV (Fig. 2m) were attributed to the π* orbital of C atoms (C1s–$\pi^*_{C=C}$) connected to either C or H sites from unsaturated hydrocarbons or olefins and to unsaturated C bonds in the ring structures of aromatic hydrocarbons (Ade and Urquhart, 2002; Cody et al., 2008; Solomon et al., 2009). These results are in line with Keiluweit et al. (2010) who demonstrated that increased charring temperature during pyrolysis could lead to peak broadening between 284.0 and 285.0 eV and to an increase in aromatic C compared to aliphatic and O-containing C due to an increasingly condensed nature of black C in char. Similar results were also reported for vitrinite by Cody et al. (1998), graphite by Haberstroh et al. (2006), black C by Lehmann et al. (2005) and chars made from wood and grass by Heymann et al. (2011). The next higher excitation appeared with varying levels of intensity near 286.6 eV (Fig. 2m). Solomon et al. (2009) indicated that these spectral features could be attributed to the C 1s–$\pi^*_{C=C}$ transitions of aromatic C connected to O atom (C–OH) in phenols and the C 1s–$\pi^*_{C=O}$ transitions from carbonyl substituted aromatic structures of quinones, phenols and ketones (Cody et al., 1998; Haberstroh et al., 2006; Braun et al., 2007). The C 1s absorption bands of the investigated pyrogenic structure near 287.6 eV were separated from the first lowest π* energy transitions by greater than 2.9 eV (Fig. 2m). Cody et al. (1998, 2008) indicated that absorption in this energy range is usually attributed to the 1s–$\sigma^*/3p_{C-H}$ transitions due to aliphatic hydrocarbons (Table 1). However, Haberstroh et al. (2006) demonstrated that these absorption bands could also be the results of C 1s–$\pi^*_{C=O}$ transitions from carbonyl structures of aromatic ketones. The C 1s spectra exhibited distinct peaks near the energy range of 288.3 eV reflecting the presence of C 1s–$\pi^*_{C=O}$ transitions from carboxylic/carbonyl (COOH/COO) functional groups bonded to unsaturated C species (Ade and Urquhart, 2002; Solomon et al., 2005, 2007; Cody et al., 2008). Cody et al. (1998) and Haberstroh et al. (2006) stated that aromatic or unsaturated C bonded to another C atom has a strong 1s–π* transition at about 285 eV. However, as more electron-drawing atoms such as O are added or substituted in organic molecules, binding energy of C 1s–π* electron increases leading to a shift in the 1s–π* transitions of aromatic C to higher energies by up to 1.9 eV for the one O atom present in the case of phenols or by up to 3.9 eV for the two O atoms bonded to C in the case of carboxylic functionalities associated with char and coal. Similar results were also reported by Solomon et al. (2009) for mono, di and tricarboxylic acid containing compounds. The C K-edge absorption bands near 289.7 eV (Fig. 2m) could be ascribed to spectral features associated with 1s–3p/σ^*_{C-OH} transitions of alcohols and hydroxylated- and ether-linked C species (Table 1; Ishii and Hitchcock, 1988; Sham et al., 1989). These spectral features could also be due to bands associated with C 1s–$\pi^*_{C=O}$ transition of carbonyl structures (R–COOH), *sp3* hybridized C from aromatic alcohols and higher-lying π* orbital of C from aromatic ring structures connected to an O atom in the case of quinine structures (Solomon et al., 2009). Cody et al. (1998) reported that core level transitions to bound states associated with C in alcohol, ether, methyl and methylene functionalities do occur

and the excited state is generally considered to be a state involving mixed C 1s–$\sigma^*/3p_{C-H}$ (Rydberg-like) characteristic (Stöhr, 2001).

3.1.2. Nano-scale cluster analysis of C from the organomineral interface

The C K-edge cluster maps showing the inner, intermediate and outer regions of the organomineral interface were presented in Fig. 2g–l. The spectra collected from the inner interface (Fig. 2g–h) were dominated by broad but intense resonances near 284.5 and 285.3 eV (Fig. 2n). However, these resonances were either weakly developed or present as a shoulder in the spectra collected from the intermediate interface (Fig. 2i–k) or absent in the outer interface of the organomineral region (Fig. 2l). Due to the proximal position of the inner interface to the pyrogenic structure and the similarity of the spectral signatures collected from this region to that of the black C particle, the C 1s transitions near 284.5 eV in the case of the inner interface spectra could be largely from low-energy π* absorption bands associated with quinine, benzene or diene structures (Kolczewski et al., 2006). Similarly, the transitions near 285.3 eV could also be related to the π* orbital of C atoms characteristic of C–H sites or to unsaturated C bonds (C═C) in the aromatic ring structures (Brandes et al., 2004; Lehmann et al., 2005; Solomon et al., 2005). However, the weakly developed resonances observed in the intermediate and outer regions spectra of the organomineral interface (Fig. 2i–l) near 284.5 and 285.3 eV (Fig. 2m) seem to be more likely the results of π* orbital of C atoms from aromatic structures of non-black C organic matter sources (Table 1; Solomon et al., 2009). Boese et al. (1997) and Kaznacheyev et al. (2002) reported that these resonance could also arise from the C 1s–$\pi^*_{C=C}$ transitions of aromatic ring structure associated with aromatic amino acids and nucleobases. The prominent shoulders near 286.5 eV (Fig. 2n) of the spectra collected from the inner, intermediate and outer interfaces (Fig. 2g–l) could be ascribed to the C 1s–$\pi^*_{C=C}$ transitions of C bonded to O atoms (C–OH) of phenols and to C 1s–$\pi^*_{C=O}$ resonances from carbonyl substituted aromatic structures of ketones and phenols (Cody et al., 1998; Haberstroh et al., 2006; Braun et al., 2007). However, in the intermediate and outer regions of the organomineral interface (Fig. 2i–l) these transitions could also be the results of the C 1s–$\pi^*_{C=C}$ and C 1s–σ^*_{C-N} transitions of amide-C in pyrrole side ring structures (C═C–N) of microbial amino acids and nucleobases and the C 1s–$\pi^*_{C=N}$ transition of C=Nx species of organic matter originating from non-pyrogenic C sources (Table 1; Kaznacheyev et al., 2002; Samuel et al., 2006; Solomon et al., 2009). The C absorption bands that emerged near 287.5 eV (Fig. 2n) from the inner interface of the organomineral complex could most likely be from the $1s–\sigma^*/3p_{C-H}$ transitions due to aliphatic hydrocarbons and from the C 1s–$\pi^*_{C=O}$ transitions from carbonyl structures from aromatic ketones related to the nearby particulate black C particle (Cody et al., 1998; Solomon et al., 2009). However, the prominent shoulders and the sharp resonances that appeared near 287.5 eV from the intermediate and outer interface spectra seem to be the results of C 1s–σ^*_{C-H}/3p Rydberg-like excitations of CH_3, CH_2 and CH aliphatic-C forms that may form non-polar termini and could confer hydrophobic properties to organomineral interface. Kinyangi et al. (2006) and Solomon et al. (2009) suggested that these resonances could also arise from the π* transitions of imine C (C═N) related to imidazole rings structures of amino groups, nucleobases and other re-synthesized microbial residues present in the organomineral region. Kaznacheyev et al. (2002) pointed out that peaks around this energy point may not be from a single state rather they could be manifestations of a number of unresolved C 1s–π* transitions of C atoms or they could also be contribution from the σ^*_{C-H} states forming broad bands instead of individual peaks. The NEXAFS spectra from the various organomineral interface regions exhibited multiple peaks near 288.1 eV in the fine structure of the C K-edge indicating the presence of multiple organic C moieties (Fig. 2n). The C 1s resonances near 288.1 eV from the inner interface (Fig. 2g) could be primarily attributed to the C 1s–$\pi^*_{C=O}$ transitions of carboxylic/carbonyl ($COOH/COO^-$) structures and to a lesser extent to the C 1s–$\pi^*_{C=C}$ transitions of ring structures associated with aromatic carboxylic acids, aromatic alcohols stemming from the black C (Table 1; Francis and Hitchcock, 1992; Schäfer et al., 2005). These suggestions are in line with the results of Shafizadeh and Sekiguchi (1983) who stated that during oxidative degradation of black C-rich materials such as char and coal, polycyclic or substituted aromatic centers could be converted to aromatic carboxylic acids. Solomon et al. (2009) also reported that these aromatic carboxylic acids exhibit a well-defined absorption peak near 288.5 eV reflecting the C 1s–$\pi^*_{C=O}$ transition of carboxyl functional groups bonded to unsaturated C. Haumaier and Zech (1995) and Glaser et al. (1998) indicated that these aromatic carboxylic acids signify the presence of pyrogenic C in environmental samples and can be used as molecular markers for black C. However, the resonances exhibited near 288.1 eV from the intermediate and outer interfaces of the organomineral region (Fig. 2g–k) could also be the results of C 1s–$\pi^*_{C=O}$ transitions of the aldehyde functionalities of deoxyaldohexoses and from the C 1s–$\pi^*_{C=O}$ transitions of carboxylic-C (COOH) functionalities related to polysaccharide structures (Braun et al., 2007; Solomon et al., 2009). In addition, the C 1s–$\pi^*_{C=O}$ resonances characteristic of carboxylic-C functionalities from amino sugars, amino acids and contributions from the C 1s–σ^*_{C-N} transitions of amide (CONH) functionalities from non-black C organic matter sources present in association with the black C and mineral matter could also contribute to these peaks (Zubavichus et al., 2005; Solomon et al., 2009). These suggestions are supported by the results of Kaznacheyev et al. (2002) who demonstrated that the carboxyl peak positions of some amino acids could be lowered by up to 0.4 due the substitution of the –OH group in the carbonyl structure of some amino acids by $-NH_2$ group. Such substitution might influence the location of the C 1s–$\pi^*_{C=O}$ transitions and could lower the energy peak by up to 0.3 eV to 288.3 eV for example in the case of asparagine or by up to 0.4 eV to 288.2 eV in the case of glutamine due to the differences in electronegativity of $-NH_2$ compared with –OH and the oscillator strength of the $\pi^*_{C=O}$ orbital (Hitchcock and Ishii, 1987; Kaznacheyev et al., 2002; Solomon et al., 2009). The presence of these organic structures in the organomineral complex is of particular importance since Kinyangi et al. (2006) demonstrated that microbial organic matter with protonated (H_3N^+) and deprotonated (COO^-) termini could interact with the black C and mineral surfaces and could form surface coatings or thin film-type layers through a variety of adsorption processes. Chenu (1995) and Chenu and Stotzky (2002) suggested that such microbial-derived exudates are susceptible to rapid and irreversible adsorption by clay minerals mainly through van der Waals forces and hydrogen bonding. Pignatello et al. (2006) and Joseph et al. (2010) also indicated that numerous mechanisms including hydrogen bonding, cation-bridging, covalent bonding and hydrophobic interactions could be involved in the associative interactions and subsequent binding of non-black C organic compounds to pyrogenic carbonaceous structures such as char. The C K-edge spectral signatures observed near 289.9 eV from the inner interfaces of the investigated organomineral complex could be from the higher-lying π* orbitals (C 1s–$\pi^*_{C=O}$) of C atoms of aromatic ring structures connected to O as in the case of quinones. These spectral features could also be due to absorption bands associated with the C 1s–$\pi^*_{C=O}$ transitions of carbonyl structures or *sp3* hybridized C of aromatic alcohols originated from the pyrogenic structure present in this sub-micron-C repository environment (Table 1). However, the sharp absorption bands observed near 289.9 eV from the intermediate and exterior regions could be from the C 1s–3p/σ* transitions of O-alkyl (C–OH) molecular orbital of polysaccharides and amino sugars (Table 1). In addition, they could also be contribution from the $\pi^*_{C=O}$ resonances associated with carbonyl structures (HNCONH) related to nucleobases (Samuel et al., 2006) from non-black C organic matter sources

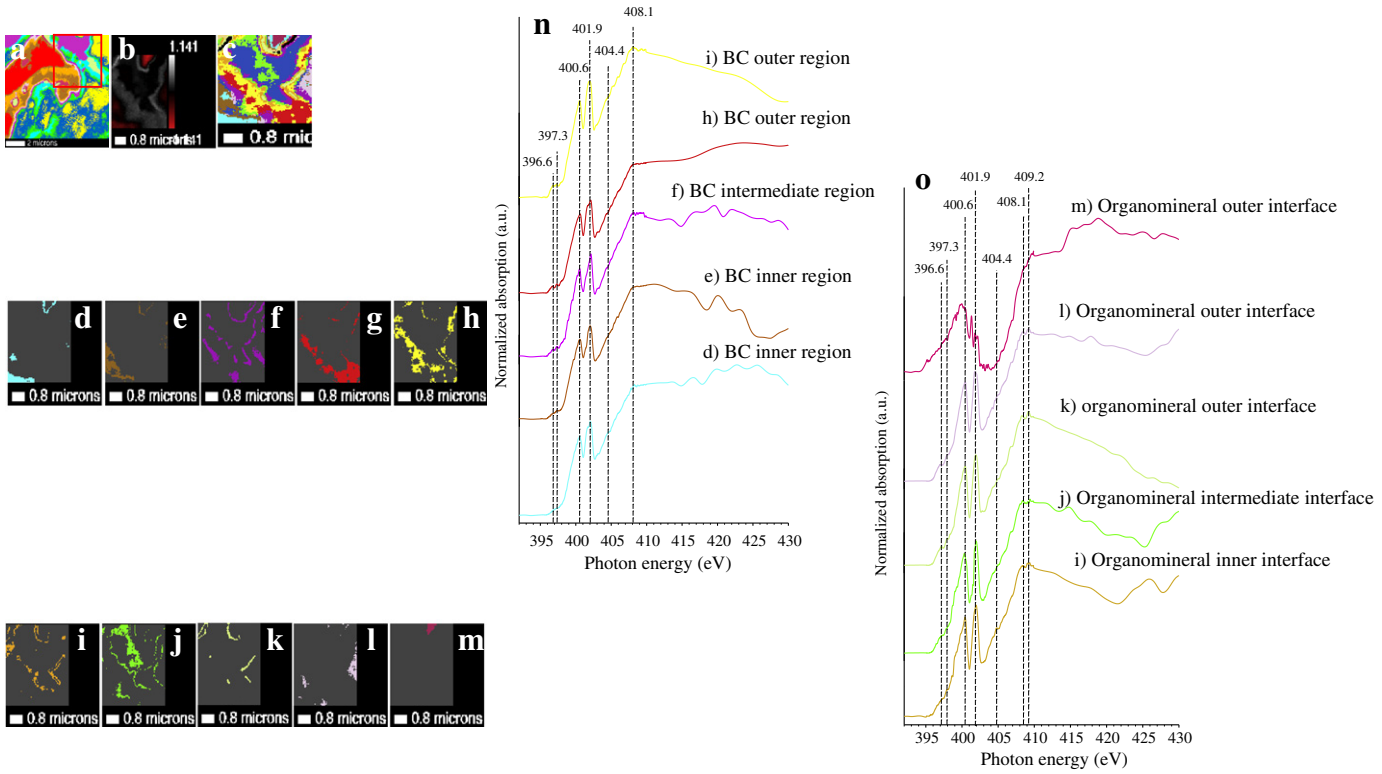

Fig. 3. High-resolution spatial images showing cluster map of C (a in red box showing the area from which the remaining element-specific NEXAFS data recorded), composition thickness map (b) and cluster index (c) maps and submicron-scale N cluster images of the black C (d–h) and organomineral interface (i–m) regions and their respective N NEXAFS spectra (n–o). (For interpretation of the references to color in this figure legend, the reader is referred to the web version of this article.)

present in association with the pyrogenic C and mineral matter in the intermediate and exterior regions of the organomineral interface. Samuel et al. (2006) and Solomon et al. (2009) indicated that the $\pi^*_{C=O}$ peak from nucleobases, which are building blocks of (deoxy) ribonucleic acids, normally appears near 286.6 eV. However, Boese et al. (1997) and Kaznacheyev et al. (2002) showed that due to the inductive effect of N on the neighboring atoms the signals for these transitions could shift significantly and appear near 288.1 eV if the N atom is attached to the carbonyl structure (O═C–NH) or it may rise at an even higher-energy range (e.g., 289.5 eV) if two N atoms are present in the carbonyl (HNCONH) structures.

3.2. N K-edge STXM–NEXAFS spectromicroscopy

The high-resolution N K-edge STXM–NEXAFS composition thickness map (Fig. 3b) map revealed black C (dark red) and organomineral (light gray) dominated regions in the investigated organomineral assemblage. The N K-edge cluster indices map (Fig. 3c) demonstrated the various micro- and nano-repository environments resent in the black C (Fig. 3d–h) and the organomineral interface (Fig. 3i–m) regions. The experimental N NEXAFS spectra collected from these regions (Fig. 3n–o) exhibit three distinctively discernable and well-resolved principal resonance regions. According to Fig. 3n and o, the first energy band occurred in the 396.0–399.0 eV energy range, while the second resonance appeared between 400.4 and 404.4 eV. The third region consists of broad transitions between 406.5 and 409.8 eV. The sharp absorption bands between 396.0 and 404.4 eV were primarily due to the π* orbitals (N 1s–π*) occurring at lower energies and represent the electronic transitions of N atoms from 1s to different π* levels. The higher-energy broad resonances between 406.5 and 409.8 eV were related to the σ* shape resonances of N atoms (N 1s–σ*) from the black C and organomineral regions indicating the presence of numerous N functionalities in the investigated micro- and nano-C repository environments (Mitra-Kirtley et al., 1993a,b; Vairavamurthy and Wang, 2002).

3.2.1. Nano-scale cluster analysis of N from the black C

The stacked N K-edge spectra collected from the outer, intermediate and core regions of the pyrogenic structure (Fig. 3d–h) exhibited multiple peaks near 396.6 and 397.3 eV (Fig. 3m). These weakly developed resonances could primarily be indications for the presence of N 1s–π* transitions from pyridinic-N groups, a six-ring heterocyclic N compounds with C–H group replaced by 1 N atom. These results are in agreement with the energy positions reported by Mitra-Kirtley et al. (1993a,b), Pels et al. (1995) and Vairavamurthy and Wang (2002) for a variety of pyridinic-N derivatives present in pyrogenic structures. Leinweber et al. (2007) also showed that despite differences in chemical structures of pyridine analogues the first lower-energy N 1s–π* peaks of pyridine molecules usually appear near the above mentioned energy ranges. However, Leinweber et al. (2007) surmised that there is also a chance that the lowest energy N 1s–π* resonances observed in the 398.7 to 399.9 eV energy range could be from pyrazole, imidazole, pyrazine, pyrimidine or even nitrile functionalities present in the pyrogenic structures. The intense N 1s–π* transitions recorded near 400.6 eV from the various regions of the particulate black C particle could be principally attributed to the π* resonance energy of pyridones, a six-ring heterocyclic N molecules with a hydrogen atom bound to 1 N atom and a keto group next to the N atom (Pels et al., 1995; Leinweber et al., 2007). Zhu et al. (1997) indicated that pyridone functionalities could be the results of surface oxidation of highly reactive microporous carbonaceous materials such as char. However, Mitra-Kirtley et al. (1994) and Leinweber et al. (2007) suggested that there could also be minor contributions to this peak from spectral features related to the π* resonances of pyridinium N moieties, a protonated pyridinic-N compound that usually occurs at a higher-energy resonances than pyridine π* resonances. Moreover, these authors pointed out that π* orbitals occurring near this lower

energy band could also be an indication for the presence of pyrroles due to the similarity of the chemical environment of the N atom present in pyridones and pyrroles. Mullins et al. (1993) indicated that pyridone analogues generally have their lowest-energy π* resonances near 400.7 eV, energy position very much in line with the results of the present investigation. However, pyridones exist in two tautomers (carbonyl and zwitterion), with the carbonyl form as the most abundant structure in pyrogenic materials and the chemical environment of the N atom in this tautomer is very similar to the N in five-membered unsaturated heterocyclic compounds such as pyrroles. Hence, theoretically there is a very good chance that the π* peak location of these two N structures i.e., pyridones and pyroles could overlap (Mitra-Kirtley et al., 1994; Vairavamurthy and Wang, 2002). Nonetheless, Mullins et al. (1993) suggested that the π* peak of pyridone could be slightly shifted to lower energy compared to that of pyrrole structures, perhaps due to the interaction of the carbonyl groups with the aromatic systems. Therefore, there is a strong possibility that the intense and well separated N 1s–π* peaks observed from the investigated pyrogenic C near 400.6 eV could be primarily from pyridone structures. The broad but well separated N 1s–π* transitions observed near the 401.9 eV energy position adjacent to the pyridone peak (Fig. 3n) could be mainly due to the spectral features arising from pyrrole analogues — five-ring heterocyclic aromatic N compounds present in the particulate black C structure. These results are in agreement with the π* resonance peak positions obtained from pure pyrrole derivatives such as carbazole or from pyrrolic-N present in imidazoles, pyrazoles, pyrimidines and purine structures (Leinweber et al., 2007). Mullins et al. (1993) pointed out that the energy position of the π* transitions is determined in part by the orbital description of the lone pair of electrons at the N site and that the π* resonance increases with increasing effective nuclear charge or decreasing electron density on the absorbing atom. The N atom in pyridine has its lone pair unshared in the sp^2 orbital. Thus it is slightly negatively charged and the lowest-energy π* resonance also occurs at a lower energy as shown in the present investigation. However, the N atom in pyrrole analogues has the lone pair delocalized in the pz orbital, which is involved in the π* cloud of the aromatic system that decreases electron density from the N site (Mullins et al., 1993). Therefore, pyrroles usually carry a lower electron density. Consequently the π* resonance of pyrrole molecules exhibits a higher-energy π* resonance appearing at higher-energy positions than pyridine and pyridone molecules (Mullins et al., 1993; Leinweber et al., 2007). The nano-scale cluster analysis of N forms of the particulate black C present in the submicron-C repository environment also revealed a series of weak π* resonance features near 404.4 eV. These spectral features could be attributed to the presence of aromatic amines in the investigated pyrogenic C structure (Mullins et al., 1993). Similar results were reported by Mitra-Kirtley et al. (1994) using N XANES spectroscopy studies of coal. The broad spectral features observed near 408.1 eV could be due to the main N 1s–σ* transitions of saturated amines. Mitra-Kirtley et al. (1994) demonstrated that π* resonances are largely absent in saturated amine spectra and that resonance which appear near 408.0 eV are largely the results of σ* transitions. However, there is a possibility that these broad spectral features could also be the result of higher-energy N 1s–σ* transitions related to pyridinic, pyrrolic, pyridonic and nitril N functionalities present in the investigated pyrogenic C particle (Leinweber et al., 2007). These suggestions concur very well with the results of Zhu et al. (1997) who investigated the fate of N functionalities during pyrolysis of N-containing reference compounds and demonstrated that saturated amines only show σ*-shaped resonances, while aromatic N-containing molecules have both π*- and σ*-shaped resonances.

3.2.2. Nano-scale cluster analysis of N from the organomineral interface

The N K-edge spectra collected from the inner, intermediate and outer (Fig. 3o) regions of the organomineral interface revealed multiple peaks near the 396.6, 397.3, 400.6, 401.9, 404.4, 408.1 and 409.2 eV energy positions. The resonances near 396.6 and 397.3 eV were attributed primarily to the N 1s–π* transitions of amines and amides originating possibly from amino acids and amino sugars present in the organomineral complex in various levels of association with the particulate black C and mineral matter (Zhu et al., 1997; Vairavamurthy and Wang, 2002; Leinweber et al., 2007). This suggestion is in agreement with the assessment of the C K-edge NEXAFS spectra recorded from the organomineral interface regions. Amino acids serve as energy sources for soil microorganisms and as major components of the soils organic N pool and their presence in non-living organic matter present in mineral soils is credited to the breakdown of native proteins derived from plants, animals, and microorganisms (Solomon et al., 2009). Amino sugars on the other hand are derivatives of monosaccharides where one or more of the nonglycosidic hydroxyl groups are replaced by an amino group ($-NH_2$). They are major constituents of bacterial and fungal cell walls and serve as structural polymers in exoskeleton of arthropods and other soil invertebrates. Both organic species (i.e., amino sugar and amino acids) are credited to play functional roles related to soil aggregation (Benner and Kaiser, 2003). However, these spectral features could also originate from aromatic – C═N – from non-black C organic matter sources and from the nearby particulate pyrogenic carbonaceous particle present in the organomineral interface (Zhu et al., 1997; Zubavichus et al., 2005). Similar results were reported by Leinweber et al. (2007) from N K-edge NEXAFS spectra of heterocyclic N compounds with pyrimidine or purine derivatives. Kruse et al. (2011) also demonstrated that the N XANES spectra of pure histidine, chitin and solid residues obtained from the step-wise offline-pyrolysis of glycyl-L-aspartic acid-spiked soil exhibited 1s–π* resonances in these energy ranges. The N 1s–π* transitions near 400.6 eV could be manifestations of such nitrogenous compounds as amino acids in organomineral interface (Fig. 3o). This is in agreement with the results of Zubavichus et al. (2005) and Leinweber et al. (2007) who indicated that amino acids with both basic and aromatic side chains, as well as organic structures with nitrile groups exhibit π* resonances around 400.0 eV. These results might be an indication that the protonated and deprotonated termini of these proteinaceous non-black C organic compounds could either interact directly with the black C and mineral matter in a "two-way" association or serve as a binding link between these two adsorbing matrices (i.e., the black C and mineral matter) in an indirect "three-way" association and lead to the retention of these organic biomolecules in the pyrogenic C dominated submicron-C repository environment. However, the N 1s–π* resonance near 400.6 eV could also be attributed to the presence of heterocyclic N compounds with imidazole, pyridine, pyrimidine and nitrile (R – C≡N) structures originating from both pyrogenic and non-pyrogenic organic matter sources and present in association with the mineral matter (Mitra-Kirtley et al., 1994; Leinweber et al., 2007). The intense π* resonances observed near 401.9 eV from the spectra of the inner, intermediate, and outer regions of the organomineral interface (Fig. 3o) could be attributed to amine structures from amino sugars and amino acids, from amide, imidazole, indole and guanidine structures of amino acids and from the π* resonances of oxidized pyridine, pyrimidine and purine based heterocyclic N compounds originated from non-black C organic matter (Vairavamurthy and Wang, 2002; Zubavichus et al., 2005; Samuel et al., 2006). These results are in accordance with our interpretation of the C K-edge spectral signatures from this micro- and nano-repository environment and support our conclusion that part of the organic matter encountered in this pyrogenic C dominated organomineral interface originated possibly from non-pyrogenic organic matter sources such as microbial exudates and breakdown products of biological membranes. The sharp N 1s–π* spectral features near 401.9 eV could also belong to pyrrolic-N from heterocyclic N structures such as pyrazine analogues related to the particulate black C

particle present in the organomineral complex (Schulten and Schnitzer, 1998; Leinweber et al., 2007). The low energy shoulders that emerged near 404.4 eV in the spectra recorded from the organomineral complex could be attributed to the N 1s–π* transitions of aromatic amine derivatives present in the particulate pyrogenic carbonaceous structure dominated submicron-C repository environment (Mullins et al., 1993; Leinweber et al., 2007). Leinweber et al. (2007) suggested that these energy positions could also arise from the π* resonance of a class of organic compounds containing N in the nitro and nitroso functional groups, while Vairavamurthy and Wang (2002) indicated that these peaks might represent highly oxidized forms of N since their energy position is the farthest among the π* resonances. These authors also stated that the type of organic forms that fits this description includes nitrated-polycyclic aromatic hydrocarbon commonly formed during incomplete combustion of organic materials — compounds with very similar molecular structure and matrix to the investigated particulate pyrogenic carbonaceous structure. The broad spectral features near 408.1 and 409.2 eV could be related to the 1s–σ* resonances amine, amide, pyrrolic imidazole pyridine, pyrimidine and purine N-containing structures from a variety of organic compounds originating from non-black C and aromatic nitrogenous organic compounds derived from the nearby particulate black C particle. These assignments are consistent with previously reported results by Mitra-Kirtley et al. (1993a,b, 1994), Zubavichus et al. (2005) and Leinweber et al. (2007). Mitra-Kirtley et al. (1994) clearly demonstrated that the main N 1s–σ* transitions of saturated amines from pyrogenic carbonaceous structures appear in the above-mentioned energy range. Similarly, Zubavichus et al. (2005) and Leinweber et al. (2007) showed that the spectra of the majority of amino acids are dominated by broad N 1s–σ^*_{N-C} peak extending from 405.6 to 409.0 eV. These authors showed that in the case of amino acids such as proline and hydroxyproline, this broad peak could apparently split into two components near 405.6 and 409.7 eV due to saturated N heterocycles. Samuel et al. (2006) and Leinweber et al. (2007) revealed that these spectral features could also be an indication for the presence of amines and amide functionalities, as well as from π* resonances of heterocyclic N compounds associated and purine structures of nucleobases. Leinweber et al. (2007) and Gillespie et al. (2008) indicated that the broad high energy peaks around 406.0 eV could be assigned to the N 1s–σ* transitions originating from mineral N compounds such as ammonium sulfates ($(NH_4)_2SO_4$), ammonium phosphate ($(NH_4)_3PO_4$) and Ca nitrates ($Ca(NO_3)_2$). However, since the N XANES spectra in the present experiment were collected from a submicron-C repository environment considerably enriched in organic N and also due to the fact that inorganic N generally represents <5% of total N in mineral soils (Schulten and Schnitzer, 1998), it is highly improbable that the XANES spectra collected from this submicron-organic C hotspot could be considerably influenced by the signals from inorganic N. Overall the presence of N K-edge spectral signatures related to amino acids, along with other organic constituents ranging from N-containing microbial polysaccharides to protein-nucleic acids co-occurring with heterocyclic N compounds in the organomineral interface is an indication that a heterogeneous mix of complex nitrogenous organic materials might have been released into and consequently sequestered in these micro- and nano-C repository environments from a variety of N-containing sources ranging from microbial and root exudates, products of biological membrane lysis to decomposition products of pyrogenic and non-pyrogenic organic matters. Huang (2004) suggested that depending on the intrinsic nature and properties of the organic moieties present in the organomineral interface organic N-containing moieties could interact with the adsorbing surfaces through a variety of ion exchange mechanisms. Besides cation-exchange reactions, adsorption and apparent sequestration of these organic N constituents by the mineral and the black C particles may also proceed through the action of such binding mechanisms as covalent, hydrophobic, hydrogen bonding or even through weak interactions involving van der Waals forces. In addition, the pyrogenic structure may also act in parallel with the mineral matter as an adsorbent and may sorb non-ionic organic species present in the organomineral interface region limiting their accessibility leading to the preservation of these organic nitrogenous compounds in this seemingly terminal submicron-C repository environment (Accardi-Dey and Gschwend, 2002; Violante et al., 2002).

3.3. Ca L-edge STXM–NEXAFS spectromicroscopy

The Ca L-edge STXM–NEXAFS composition thickness map (Fig. 4b) and cluster indices map (Fig. 4c) exhibited micro- and nano-scale spatial variations (Fig. 4d–i) and Ca K-edge spectral features associated with the various regions of the particulate pyrogenic structure (Fig. 4m) and the organomineral interface (Fig. 4n) regions. Our results show that the experimental Ca NEXAFS spectra were generally limited to a narrow energy range between 346.9 and 354.5 eV. However, they consist a series of features that arise from internal excitations from 2p to 3d states (Buckley, 1995) and exhibited complex Ca fine edge structural features in the investigated organomineral assemblage.

3.3.1. Nano-scale cluster analysis of Ca from the black C

The Ca L-edge spectra (Fig. 4m) collected from the inner, intermediate and outer regions of the pyrogenic structure (Fig. 4d–f) revealed four principal features, with two main spin-orbit related peaks (i.e., L_3 $2P_{3/2}$ and L_2 $2P_{1/2}$) appearing near 349.2 and 352.3 eV, respectively, and the smaller crystal field peaks (i.e., L_3 $2P_{3/2}$ and L_2 $2P_{1/2}$) emerging near 348.1 and 351.5 eV, respectively (Naftel et al., 2001; Fleet and Liu, 2009). A number of smaller peaks and shoulders were also observed not only preceding the main spin-orbit related peaks but also after crystal field related peaks. Naftel et al. (2001) indicated that the origin of these multi-peak patterns is known to be the crystal field arising from the symmetry of the atoms surrounding the Ca^{2+} ion in the first coordination sphere. Our results show that the energy separation of the main (L_2 $2P_{1/2}$–L_3 $2P_{3/2}$) and crystal field (L_2 $2P_{1/2}$–L_3 $2P_{3/2}$) Ca L-edge experimental peaks were 3.0 and 3.4 eV, respectively. These values were consistent with the values reported for the 2p spin-orbit splitting of Ca metal determined for a variety of Ca standards by Naftel et al. (2001) and Fleet and Liu (2009). Examination of the main experimental Ca L_3 $2P_{3/2}$ and L_2 $2P_{1/2}$ edge features and the number, position and intensity of the smaller crystal field peaks recorded from the core, intermediate and outer regions of the black C particle seem to indicate that the nature of Ca compounds present in this pyrogenic carbonaceous structure was different from inorganic Ca compounds such as Ca carbonate polymorphs ($CaCO_3$), (ferroan) dolomite-structured carbonates ($CaMg(CO_3)_2$) and Ca sulfides (CaS) (Naftel et al., 2001; Politi et al., 2008; Fleet and Liu, 2009; Obst et al., 2009). This is especially true for the L_3 $2P_{3/2}$ and L_2 $2P_{1/2}$ crystal field peaks, which were much less prominent than the ones recorded from $CaCO_3$Ca, $CaMg(CO_3)_2$ or CaS. Moreover, unlike the Ca and dolomite-structured carbonates and Ca sulfides where the crystal field L_2 $2P_{1/2}$ peaks are well split, the L_2 $2P_{1/2}$ crystal field peaks recorded from the particulate black C particle were shifted closer to the main peaks and appear as if they are extensions or shoulders of the main spin-orbit related L_2 $2P_{1/2}$ peaks. However, these features appear to indicate that the Ca L-edge spectral signatures from the investigated pyrogenic structure are much more analogous with the spectra recorded from Ca present in Ca phosphate compounds. Politi et al. (2008) demonstrated that the absence or appearance of less intense L_3 and L_2 crystal field peaks closer to the main L_3 and L_2 peaks where they appear as shoulders in the Ca absorption line-shapes is an indication for the presence of disordered or amorphous forms of Ca structures, while the splitting of the

main L_3 and L_2 peaks and appearance of a more pronounced and equally intense L_3 and L_2 crystal field peaks are an indication of the well developed crystalline Ca phase structures. Therefore, it is possible to suggest that the Ca phosphate compounds present in micro- and nano-structures of the particulate black C structures were more of a disordered nature and exhibit a similar Ca site structure with the Ca present in more amorphous Ca phosphate phases ($Ca_3(HPO_4)_2 \cdot \chi H_2O$) often found in such environmental matrices as black C rich Amazonian Dark Earths, chicken manure and bones (Naftel et al., 2001; Sato et al., 2005, 2009; Mahamid et al., 2010).

3.3.2. Nano-scale cluster analysis of Ca from the organomineral interface

The Ca L-edge spectra (Fig. 4n) collected from the inner, intermediate and outer regions of the organomineral interface (Fig. 4g–i) revealed intense main spin-orbit related peaks L_3 $2P_{3/2}$ and L_2 $2P_{1/2}$ near 349.2 and 352.2 eV, respectively, similar to the pyrogenic structure. However, the crystal field L_3 $2P_{3/2}$ and L_2, as well as the peaks preceding L_3 $2P_{3/2}$ were more distinctive in appearance and well separated from the main L_3 $2P_{3/2}$ and L_2 $2P_{1/2}$ peaks compared to the corresponding peaks observed from the black C structure. In addition, the L_2 $2P_{1/2}$ crystal field crystal peaks also seem to have shifted slightly to lower energy. The splitting of the main L_3 and L_2 peaks and appearance of a more pronounced L_3 $2P_{3/2}$ and L_2 crystal field peaks indicate the presence of a more transient and relatively more crystalline phases of Ca compounds (Politi et al., 2008) in the investigated organomineral interface. These Ca compounds could either be inorganic Ca phosphates or Ca-containing organic compounds sorbed or present in various forms of associations with the pyrogenic carbonaceous structure and the mineral matter. The possible sources of Ca-containing organic compounds observed in the organomineral complex could be Ca-containing exoenzymes, Ca-containing organophosphates compounds or low molecular weight organic acids such as oxalates produced by soil fungi and known to interact particularly with metal ions such as Ca forming Ca oxalate polymorphs (Naftel et al., 2001). The inorganic Ca compounds present in the organomineral complex could be mixtures of a more transient and crystalline phases of Ca compounds such as tri ($Ca_3(PO_4)_2$) and octa ($Ca_4H(PO_4)_3 \cdot 2.5H_2O$) Ca phosphates and hydroxyapatite ($Ca_5(PO_4)_3(OH)$) (Naftel et al., 2001; Benzerara et al., 2004; Fleet and Liu, 2009). These results seem to further indicate that there are no identifiable contributions from intermediate and extended structural chemistries of calcite, dolomite and Ca-containing sulfides to the compositional chemistry of Ca present in the investigated submicron-C repository environment.

3.4. Fe L-edge STXM–NEXAFS spectromicroscopy

The high-resolution Fe STXM–NEXAFS composition thickness map (Fig. 5b) and cluster index (Fig. 5c) maps showed the different micro- and nano-regions of the pyrogenic C (dark red) and the nearby organomineral interface (light gray) regions. The stacked Fe NEXAFS spectra (Fig. 5m–n) showed the Fe L-edge signatures related to the various regions of the black-C structure (Fig. 5d–f) and organomineral interface (Fig. 5g–i). The Fe L-edge spectra revealed two distinct Fe absorption bands where the first region representing the Fe L_3 edge related to an electronic dipole transition between $2p_{3/2}$ and 3d orbitals emerged between 705.0 and 715.0 eV, while the second region showing the L_2 edge associated with an electronic transition between $2p_{1/2}$ and 3d orbitals appeared between 719.0 and 728.0 eV (van der Laan and Kirkman, 1992).

3.4.1. Nano-scale cluster analysis of Fe from the black C

The NEXAFS spectra (Fig. 5m) extracted from Fe 2p cluster maps of the core, intermediate and outer regions (Fig. 5d–f) of the pyrogenic structure exhibited well-resolved doublets at the Fe L_3- (near

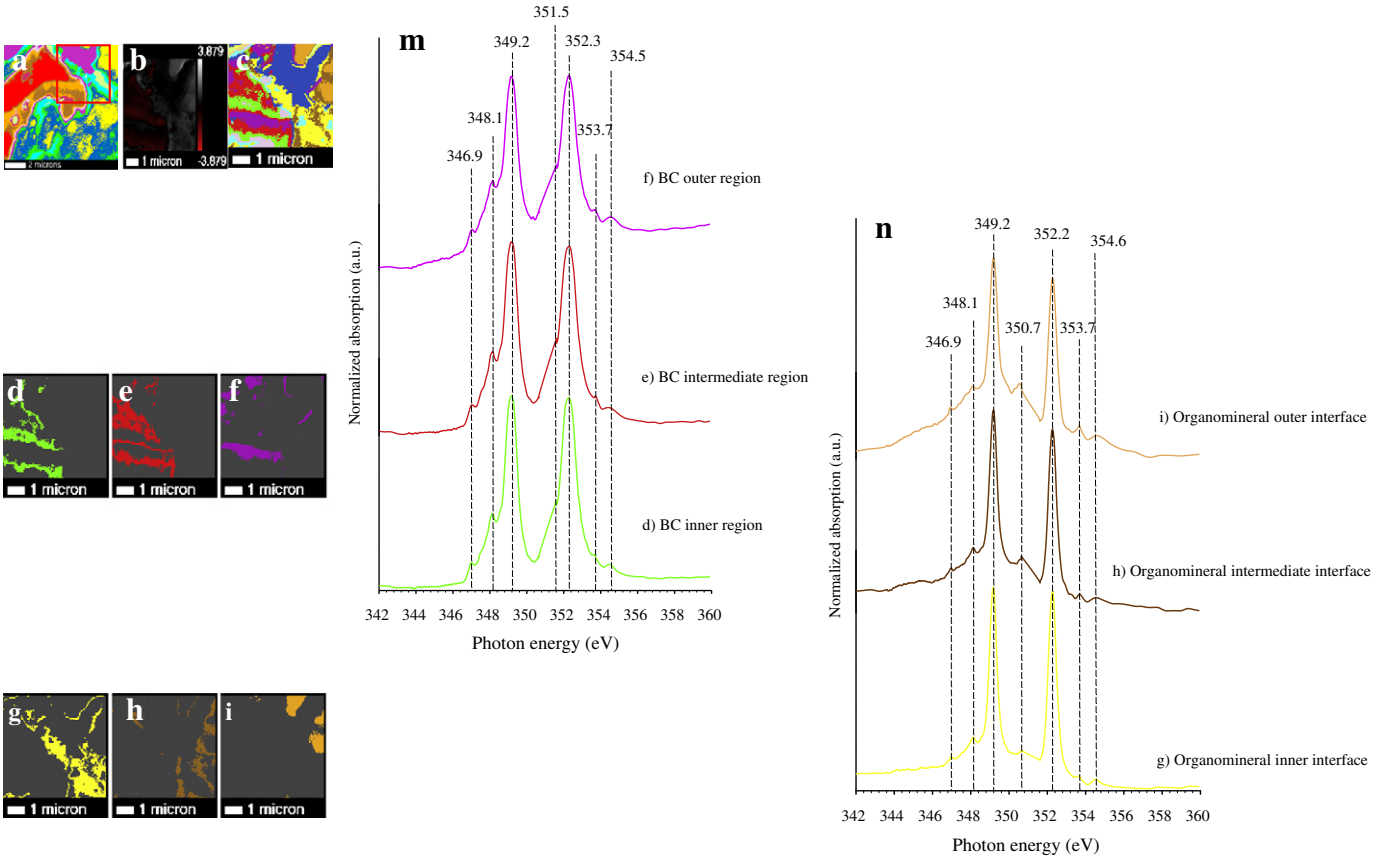

Fig. 4. High-resolution cluster map of total C (a), Ca L-edge composition thickness map (b) and cluster index (c) maps and submicron-scale cluster images of Ca associated with the black C (d–f) and the organomineral interface (g–i) regions and their respective Ca spectra (m–n).

707.9 and 709.4 eV) and L_2- (near 721.0 and 722.8 eV) edges. Our results also indicated that the Fe L_2 $2P_{1/2}$ transitions near 721.0 and 722.8 eV were less intense, broader and almost of equal magnitude, while the Fe L_3 $2P_{3/2}$ peaks near 709.4 eV were much more intense and sharp compared to the Fe L_3 $2P_{3/2}$ peaks that appeared near 707.9 eV (Fig. 5m). These results seem to suggest that the Fe chemistry of the pyrogenic structure seems to be dominated by Fe^{3+} species and the contribution of Fe^{2+} to the overall spectral signature seems to be limited (van Aken and Liebscher, 2002; Hitchcock et al., 2009). The possible sources of Fe^{3+} species in the investigated particulate pyrogenic structure could be remnant Fe species from the precursor biomaterial and sorption of soluble or colloidal Fe^{3+}-containing species on the surface or inside the porous structure of the particulate black C particle due to negative charges present on the surface of this amphiphilic pyrogenic structure. The amphiphilic nature of black C could also lead to the adsorption of negatively charged organic C functionalities including amino, carboxylic, hydroxyl and phosphate groups from non-black C organic matter sources such as microbial metabolites as indicated by our C and N K-edge NEXAFS spectroscopy on the surface of the investigated pyrogenic structure. The presence of surface reactive C functionalities in turn could render additional capacity for the black C particle to sorb positively charged metal cations such as trivalent Fe species through passive adsorption involving an electrostatic interaction between the metal cation and the negatively charged surface reactive organic C functional groups leading to the binding and accumulation of Fe^{3+} on the pyrogenic carbonaceous structure (Urrutia and Beveridge, 1994; Ledin et al., 1999).

3.4.2. Nano-scale cluster analysis of Fe in the organomineral interface

The experimental Fe $L_{3,2}$-edge NEXAFS spectra recorded from the inner, intermediate and outer regions of the organomineral interface (Fig. 5n) showed well-resolved Fe L_3 $2p_{3/2}$ signals near 707.9 and 709.4 eV, while the Fe L_2 $2p_{1/2}$ peaks appeared near 720.8 and 722.5 eV. These spectral signatures were distinctly different from spectra recorded from wüstite (FeO), hercynite ($FeAl_2O_4$) and Fe^{2+}-phosphate minerals composed exclusively of ferrous (Fe^{2+}) iron (Crocombette et al., 1995; van Aken and Liebscher, 2002; Miot et al., 2009). However, they showed a great deal of similarity with the Fe $L_{3,2}$-edge NEXAFS spectra recorded from minerals composed of ferric (Fe^{3+}) iron compounds such as hematite, (α-Fe_2O_3), goethite (α-FeO(OH)), magnetite (Fe_3O_4), schwertmannite ($Fe_3O_8(OH)_6(SO_4)$) and ferrihydrite ($Fe_5HO_8 \cdot 4H_2O$) (van Aken and Liebscher, 2002) and with the spectra of Fe^{3+}-phosphate compound recorded by Miot et al. (2009). These results suggest that the investigated metal-rich submicron-C repository environment was predominantly composed of more crystalline iron (Fe^{3+}) oxides (e.g. hematite) and iron (Fe^{3+}) oxyhydroxides (e.g. goethite). However, they also provide an indication for the presence of a less crystalline iron (Fe^{3+}) hydroxide ($Fe(OH)_3$) and oxyhydroxides (e.g. ferrihydrite) species, as well as Fe^{3+} cations in the investigated micro-organomineral assemblage. Iron compounds are commonly released in mineral soil by weathering as less ordered iron (III) hydroxides ($Fe(OH)_3$) in oxidizing situations and as dissolved Fe (II) hydroxides ($Fe(OH)_2$) in reduced conditions. These compounds will eventually dehydrate and crystallize as hematite or goethite. Hematite formation tends to be favored in warm environments, while goethite is more stable in humid and cooler environments. The presence of a more oxidized ferric (Fe^{3+}) oxide and hydroxide species in the investigated organomineral interface is, therefore, in keeping with the warm, well aerated and relatively lower pH environment of the studied soil. Our suggestions are also in agreement with the results of Violante et al. (2002) who reported that a variety of FeO(OH) and Fe_2O_3 polymorphs are commonly known to coexist as end products of advanced weathering in many tropical soils where leaching of basic cations is strong and the soil is relatively acidic. The presence of Fe oxides, hydroxides and oxyhydroxides (FeOx) in the investigated organomineral interface is very important as they are generally known to influence organic matter binding in soils evidenced by the positive correlations observed between metal and total organic C concentrations among a range of soils (Skjemstad et al., 1989). Kleber et al. (2007) also indicated that the presence of various oxides, hydroxides, and oxyhydroxides of Fe in the organomineral interface is critical for organic C binding since they can coat the surface of clay minerals (including the black C particle in this case) and provide a vast sorbent surface area or create a variety of surface types. This suggestion is in line with the results of our C and N NEXAFS results which showed the presence of proteins, nucleic acids and polysaccharides in the various regions of the metal-rich particulate black C particle and the organomineral interfaces. Urrutia and Beveridge (1994) indicated that these organic biopolymers are known to exhibit negatively charged carboxylic, phenolic, enolic, thiolate and phosphate functionalities that are highly reactive towards metal ions on account of their low isoelectric point and amphoteric nature. This could create a possibility for the Fe oxide, hydroxide and oxyhydroxide coated and/or surface charged black C and organomineral interface to interact with organic biopolymers and could lead to sequestration of organic C in the investigated submicron-C repository environment. Sollins et al. (1996) stated that the actual binding mechanism between organic C and iron oxides and hydroxides differ depending on the nature of the sorbate and sorbent present in the localized geochemical micro-scale environments and suggested that several mechanisms could play a role in the binding of C in the organomineral complex. One of the possible mechanisms for the association of organic C with the mineral and black C complex in the investigated micro- and nano-C repository environments could be sorption of negatively charged organic C from non-black C organic matter sources through replacement of surface hydroxyl groups. Lützow et al. (2006) stated that such anion exchange between simple coordinated OH groups on mineral surfaces and carboxyl and phenolic groups is one of the most important mechanism for the formation of strong organomineral associations (e.g. Fe – O – C bonds) especially in acid soils rich in minerals with protonated hydroxyl groups. Trivalent Fe^{3+} could also serve as a polyvalent cation bridge binding the negatively charged surfaces of the pyrogenic and mineral matter to the acidic functional groups of organic C present in the organomineral interface. Chenu (1995) suggested that microbial polysaccharides adsorb strongly to negatively charged mineral surfaces through polyvalent cation bridging involving iron. Complexation reactions involving organic C and Fe cations released from hydroxyl Fe surface coatings could also be additional binding mechanisms for the “two- and/or three-way” intimate association observed between the organic C, pyrogenic structure and Fe-rich mineral matrix present in the investigated organomineral interface (Wada, 1995; Huang, 2004).

3.5. Al K-edge STXM–NEXAFS spectromicroscopy

The Al K-edge STXM–NEXAFS composition thickness map (Fig. 6b) and cluster index (Fig. 6c) maps of the organomineral assemblage exhibited submicron-scale spatial distribution of Al (Fig. 6d–h) and spectral signature related with this element in the black C structure (Fig. 6i) and organomineral interface (Fig. 6j) region. The Al NEXAFS spectral signatures revealed distinct absorption bands in the energy range of 1562.8–1587.1 eV. Shaw et al. (2009) stated that these Al 1s absorption features were the results of transitions of core electrons to the first empty bond states orbitals (1s–3p) and from multiple scattering and medium-range Al order. Doyle et al. (1999), Hu et al. (2008) and Shaw et al. (2009) indicated that these Al K-edge spectra can be diagnostic for probing the bonding and symmetry of the local coordination environment around Al atoms

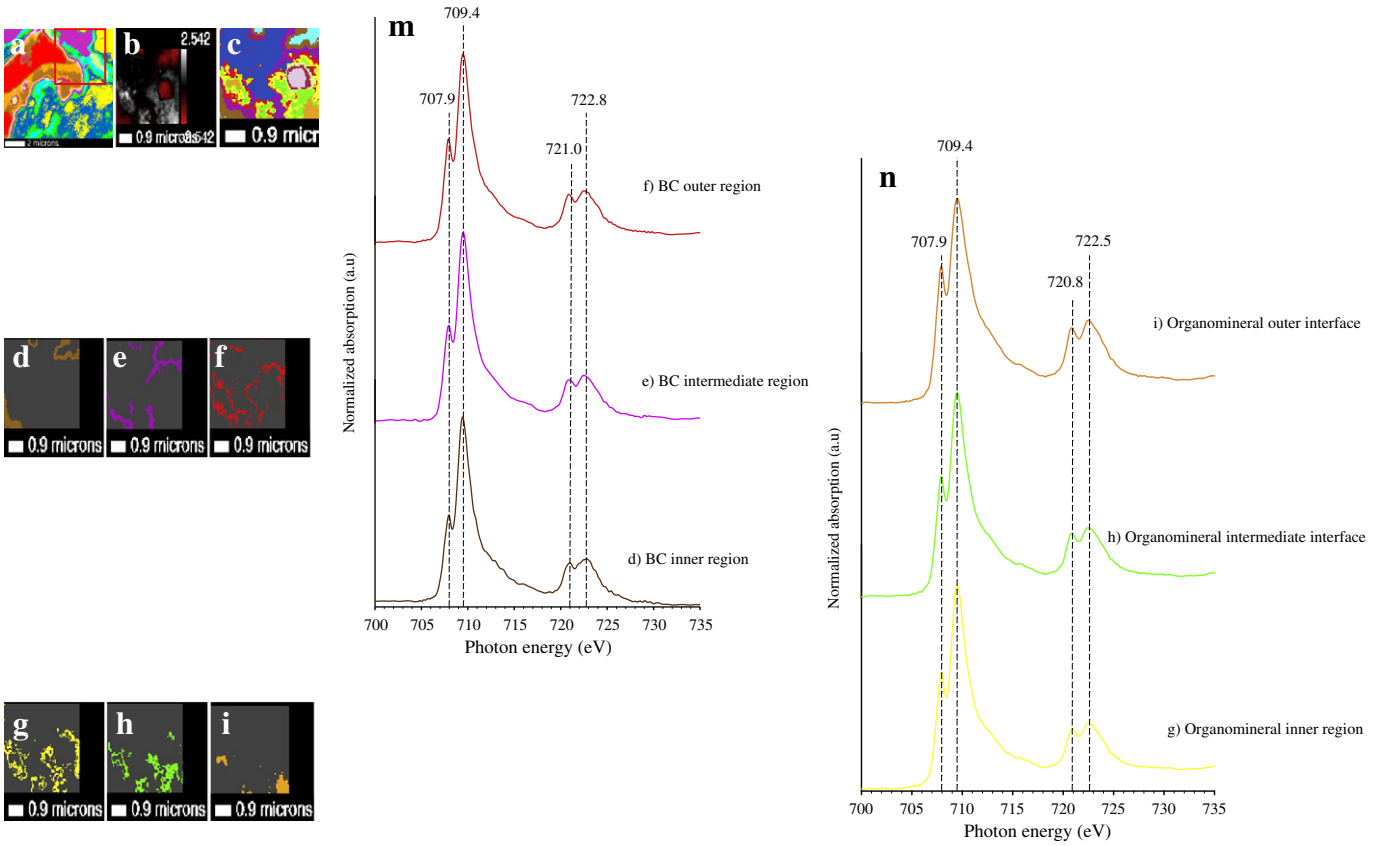

Fig. 5. High-resolution spatial cluster map of total C (a), Fe L-edge composition thickness map (b) and cluster index (c) maps and micro- and nano-cluster images of Fe associated with the black C (d–f) and organomineral interface (g–i) regions and their respective Fe NEXAFS spectra (m–n). (For interpretation of the references to color in this figure citation, the reader is referred to the web version of this article.)

and could be employed to identify diverse fine structural features related to this metal.

3.5.1. Nano-scale cluster analysis of Al from the black C

The Al 1s NEXAFS cluster maps from the outer (Fig. 6d) and inner (Fig. 6e) regions of the particulate pyrogenic structure revealed two main features near 1564.5 and 1567.2 eV with a shoulder appearing near 1570.5 eV (Fig. 6i). Additional peaks were also observed near 1578.1, 1580.0, 1582.1 and 1587.1 eV. These spectral features and energy positions were largely similar to the spectra collected from gibbsite (α-Al$(OH)_3$), Al-goethite ($Fe_{1-X}Al_XOOH$), silicate (kaolinite, $Al_4(Si_4O_{10}(OH)_8)$) and mixed metal hydroxide (hydrotalcite, $Mg_6Al_2(OH)_{16}CO_3 \cdot 4H_2O$) clay minerals (Li et al., 1995a; Ildefonse et al., 1998; Shaw et al., 2009). These Al oxides and hydroxides, as well as phyllosilicate and mixed metal hydroxide clays could coat the internal and external surfaces of the investigated particulate black C and could induce changes that modify its electrochemical properties by generating negatively and positively charge surfaces (Zhuang and Yu, 2002). Since sorption reactions are closely related to net surface charge density, the changes on charge characteristics of these coated surfaces could provide additional sorption sites and could influence the binding of metal and organic C functionalities onto the particulate black C. These suggestions are in line with Baldock and Skjemstad (2000) who indicated that the presence of Al oxides and hydroxides in soils and sediments is usually related to an increase in surface charge density, reactivity and organic C adsorptive and protective capacities of mineral surfaces.

3.5.2. Nano-scale cluster analysis of Al from the organomineral interface

The Al K-edge spectra recorded from the inner (Fig. 6f), intermediate (Fig. 6g) and outer (Fig. 6h) regions of the organomineral interface were presented in Fig. 6j. Similar to the Al 1s spectra from the particulate black C structure, the spectral signatures recorded from the inner regions of the organomineral interface were dominated by resonances similar to the structural polymorphs of gibbsite and silicate clay minerals (e.g., kaolinite) (Ildefonse et al., 1998; Yoon et al., 2004). However, the signatures from the intermediate and outer regions were distinctively different from the features recorded from the inner organomineral interface and the black C structure. These spectral features were well separated and revealed a clearly resolved main features near 1562.8, 1566.5 eV followed by a shoulder near 1570.5 eV. Moreover, additional distinct Al 1s NEXAFS spectral features were apparent near 1576.3, 1580.7, 1582.2 and 1586.7 eV. These signatures were analogous to the spectra recorded from Al oxides (e.g., corundum, α-Al_2O_3), hydroxides (e.g., diaspore) and hydrated potassium Al sulfates (e.g., K-alum, $KAl(SO_4)_2 \cdot 12H_2O$) (Ildefonse et al., 1998; Yoon et al., 2004; Hu et al., 2008; Shaw et al., 2009). Thus, our results seem to suggest that the compositional chemistry of the Al present in the organomineral interface regions was composed mostly of six-fold crystalline Al oxide and hydroxide polymorphs, where Al is present in either octahedron or dioctahedral layer. In addition, these results also seem to indicate the coexistence of Al phyllosilicate clay minerals such as kaolinite with the various polymorphs of Al oxide and hydroxides. These oxides and hydroxides of Al and mixed phyllosilicate clay minerals are known to be the common products of intensive weathering of soils present in hot and moist tropical environments as in the studied soil. The coexistence of these oxides, hydroxides and phyllosilicates in the organomineral interface is of great relevance for binding and sequestration of the various negatively charged organic C functionalities identified by our C and N K-edge NEXAFS spectromicroscopy, since these oxyhydroxide and mixed mineral communities are excellent

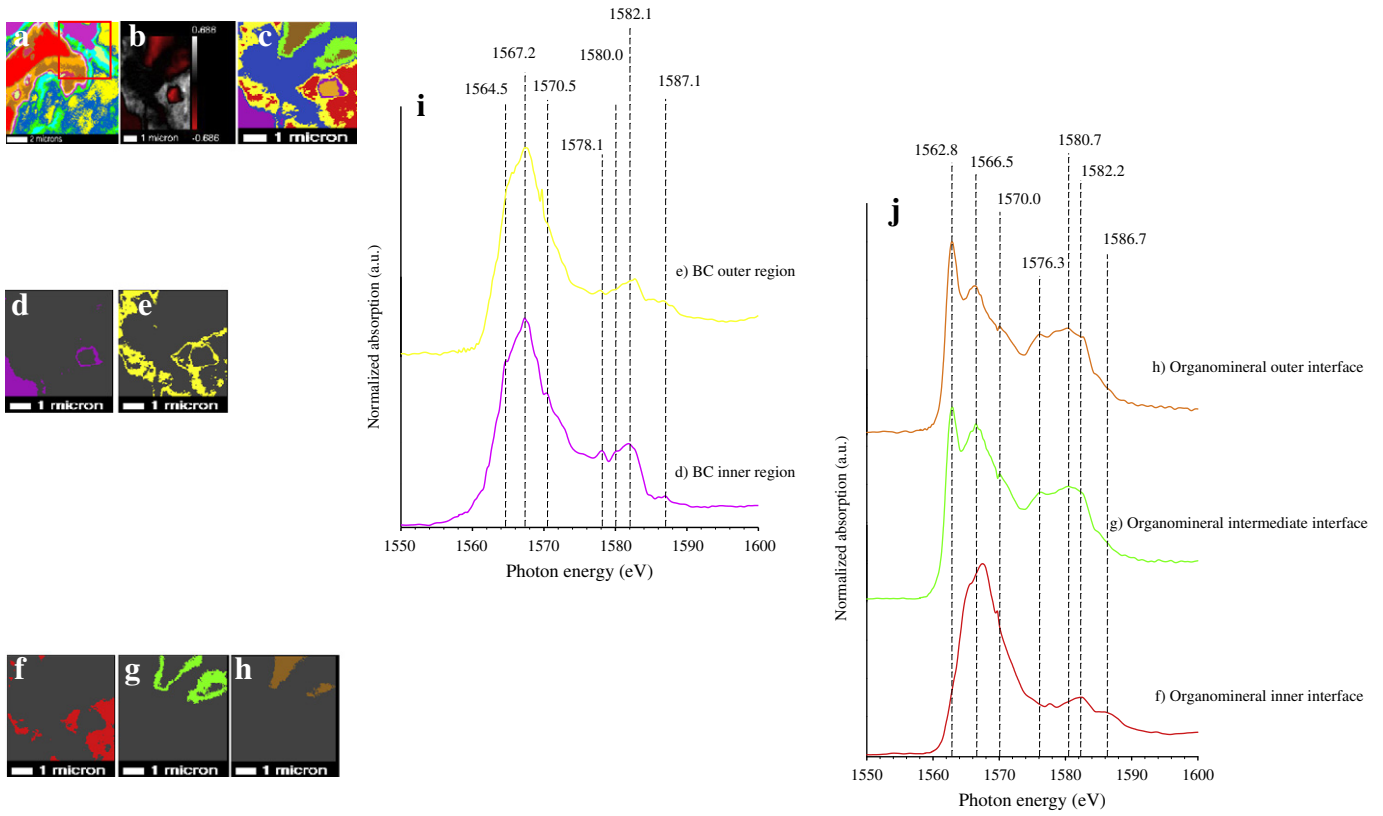

Fig. 6. High-resolution cluster map of total C (a), Al K-edge composition thickness map (b) and cluster index (c) maps and submicron-scale cluster images of Al associated with the black C (d–e) and organomineral interface (f–h) regions and their respective Al NEXAFS spectra (i–j).

sources of polyvalent cations, hydroxyl surface groups and edge sites on clay mineral and black C surfaces. Hu et al. (2008) and Lehmann and Solomon (2010) suggested that the actual sorption and binding of these organic C moieties could take place through a variety of binding mechanisms ranging from ligand exchange, polyvalent cation bridges, hydrophobic interactions and van der Waals forces to hydrogen bonding. Pignatello et al. (2006) also reported that Al^{3+}, a polyvalent metal ion abundant in tropical most soils, is known to serve as a cross-linking agent for char and non-BC organic matter such as humic acids by coordinating the acidic groups (carboxylate and phenolate) present on the surface of these organic materials, thereby providing localized high concentrations of non-black C organic matter on char surfaces. Huang (2004) also indicated that surface complexation reactions may result in the development of thick envelopes of colloidal organics on metal oxides and aluminosilicates. Chenu and Stotzky (2002) stated that the adsorption of these organic biomolecules to various surfaces could be non-reversible since it can result in conformational changes that render the biomolecules unavailable to the action of extracellular enzymes.

3.6. Si K-edge STXM–NEXAFS spectromicroscopy

The Si K-edge STXM–NEXAFS composition thickness map (Fig. 7b) and cluster index (Fig. 7c) maps of the organomineral assemblage showed the submicron-scale distribution (Fig. 7d–i) and the Si spectral signatures associated with the various regions of the pyrogenic structure (Fig. 7j) and the organomineral interface (Fig. 7k). The experimental Si K-edge spectra were well-resolved and span within the absorption bands of 1842.6 and 1864.8 eV in the Si 1s continuum revealing the existence of rich Si fine structural features (Fig. 7j–k). The intense peak that appeared near 1842.6 eV was associated with the transitions corresponding to Si ls electrons promotion of the σ* orbitals to the antibonding 3p-like (Si ls–3p) state (Li et al., 1995a; Shaw et al., 2009). Li et al. (1995a,b) indicated that these transitions are usually very strong and referred to as the Si K-edge resonances. The weak resonances which appeared between 1844.1 and 1846.8 eV and near 1852.3 eV were attributed to the multiple scattering effects from more distant atom shells, while the Si K-edge peaks that appeared near 1851.8 and 1862.9 eV were ascribed to the transitions of Si ls electrons to the e and t_2 states (Si ls–3p), respectively, and they are called symmetry-forbidden shape resonances (Li et al., 1995b).

3.6.1. Nano-scale cluster analysis of Si from the black C

The Si K-edge cluster maps showed the micro- and nano-scale distribution of Si in the inner (Fig. 7d), intermediate (Fig. 7e) and outer (Fig. 7f) regions of the black C. The Si 1s spectra collected from the pyrogenic particle (Fig. 7j) revealed intense Si K-edge features near 1842.6 eV, while additional peaks were observed near 1844.2, 1846.8, 1852.3, 1856.7 and 1864.8 eV. These spectral features resemble the Si K-edge spectra collected from Si-containing phyllosilicate ($Si_4O_{10}^{4-}$) (e.g., kaolinite, $Al_4(Si_4O_{10}(OH)_8)$, pyrophyllite ($Al_2(Si_3O_{10})(OH)_2$) and illite, $((MgCaK)_{1.52}Al_4(SiAl)_4O_{20}(OH)_4)$ and tectosilicate (SiO_2) (e.g., α-quartz, SiO_2, and microcline, $K(AlSi_3O_8)$ minerals) (Li et al., 1995b; Gilbert et al., 2003; Shaw et al., 2009). These results are in accordance with the findings of our Al K-edge spectromicroscopy of the black C structure. They also further strengthen our suggestions that these Si-containing phyllo and tectosilicate minerals are present in association with the particulate pyrogenic structure. The presence of these heterogeneous silicate clay minerals in the investigated submicron-C repository environment is very important because these minerals have a potential to

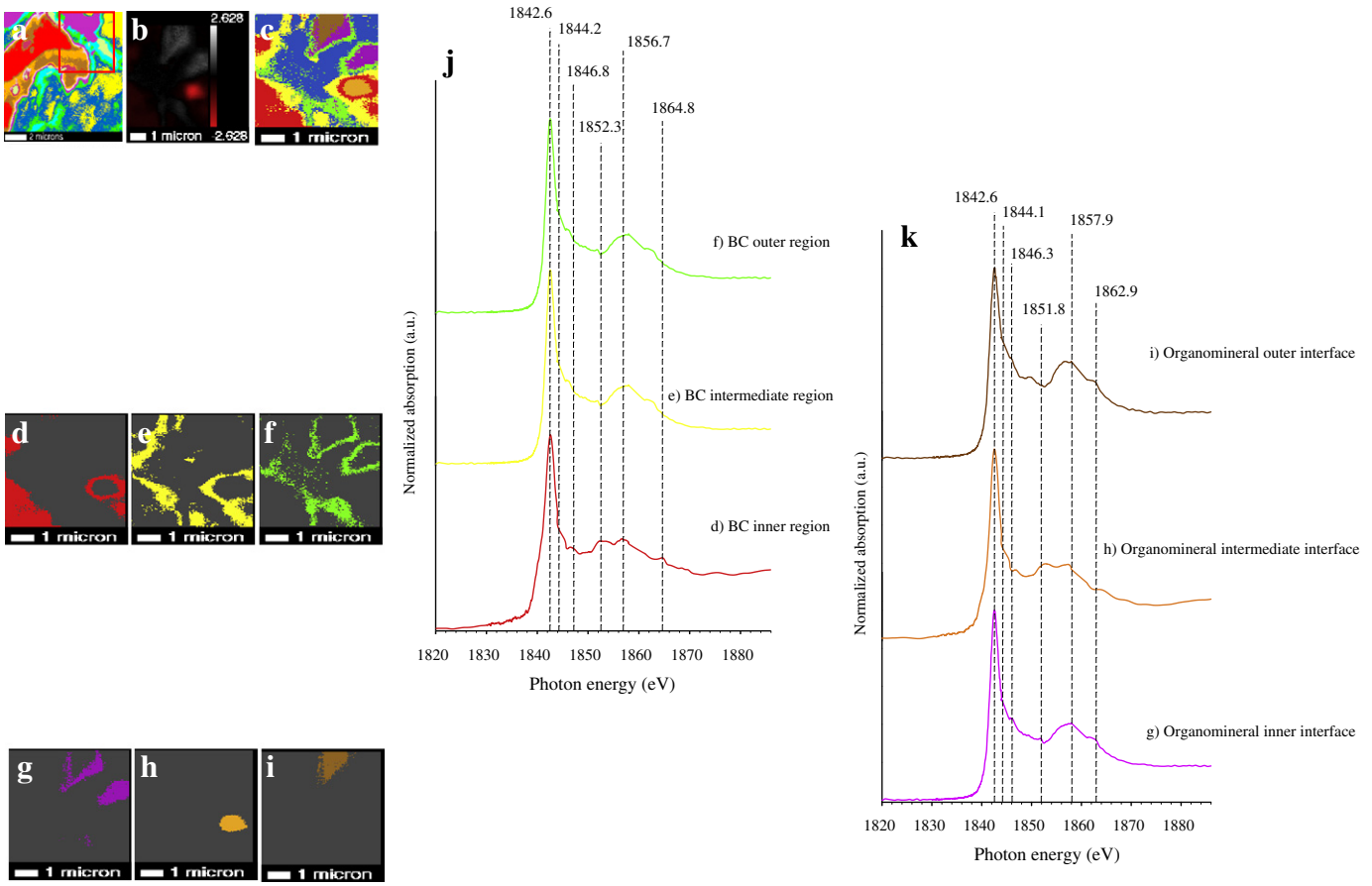

Fig. 7. High-resolution cluster map of total C (a), Si K-edge composition thickness map (b) and cluster index (c) maps and cluster images of Si associated with the black C (d–f) and organomineral interface (g–i) regions and their respective Si NEXAFS spectra (j–k).

coat the surface or porous structures of the pyrogenic particle and alter its surface charge, reactivity and its capacity to adsorb organic matter.

3.6.2. Nano-scale cluster analysis of Si the organomineral interface

The Si K-edge spectra recorded from the inner (Fig. 7g), intermediate (Fig. 7h) and outer (Fig. 7i) regions of the organomineral interface were shown in Fig. 7k. According to Fig. 7k, the most evident features of the organomineral interface spectra were the prominent Si ls–3p edge related peaks near 1842.6 eV, the Si ls-multiple scattering peaks near 1844.1, 1846.3 and 1851.8 eV and the Si ls–3p related peaks near to 1851.8 and 1862.9 eV. Li et al. (1995b) indicated that the spectral signatures near 1842.6, 1851.8 and 1862.9 eV are related to the SiO_4^{4-} cluster of Si-containing minerals in the organomineral interface. Similar to the spectra collected from the various regions of the particulate black C structure, the Si K-edge spectral features recorded from the organomineral interface also revealed a considerable similarity with the spectra collected from kaolinite, pyrophyllite and illite. They also showed some level of similarity with the α-quartz and microcline spectra (Li et al., 1995b; Gilbert et al., 2003; Shaw et al., 2009) The results from our Si K-edge NEXAFS seem to indicate that the Si compositional chemistry of the organomineral interface appears to be composed of mixed silicate clay minerals comprised for the most part of 1:1 type (kaolinite) and to a lesser extent some 2:1 type (illite) phyllosilicate clay minerals. The presence of mixed Si-containing phyllosilicate minerals in association with Fe and Al hydroxypolycations (Fe^{3+} and Al^{3+}), oxides, hydroxides and oxyhydroxides in the metal-rich organomineral interface coupled with the various organic functionalities uncovered by our multi-element NEXAFS spectromicroscopy demonstrates the tremendous sorbent and sorbate complexities in the investigated submicron-C repository environment. Sollins et al. (1996) pointed out that the specific binding mechanism between the organic C and the mineral surfaces differs depending on the nature of the observed sorbate and sorbent present in the investigated localized geochemical micro-scale environments and suggested that various mechanisms ranging from ligand exchange, polyvalent cation bridging to weak hydrophobic interactions such as van der Waals forces and H-bonding could be considered as the possible mechanisms for associations of the organic C with mineral surfaces (Vermeer et al., 1998). These authors also suggested that such adsorption reactions could provide a mechanism for protecting organic matter against biological decomposition. Huang (2004) and Sposito (2008) for example indicated that mixed phyllosilicate clay minerals and broken edges that contain hydroxylated surfaces contain silanol (Si–OH), aluminol (Al–OH) and ferrol (Fe–OH) groups. In the event of proton dissociation the silanol, aluminol and ferrol groups could develop negative surface charges. Baldock and Skjemstad (2000) also stated that these edge sites and surfaces could be involved in binding mechanisms such as ligand exchange reactions where for example the reactive inorganic protonated hydroxyl groups interact with carboxylic and phenolic groups and could lead to sorption of organic C on mineral surfaces. Hydroxypolycations and Fe and Al oxide and hydroxide precipitates present in investigated metal rich organomineral interface could also interact with the organic matter from black C and non-black C sources through various adsorption reactions that could lead to

organic C sequestration in the micro- and nano-C repository environments of the investigated organomineral assemblage.

4. Summary and outlook

The present study is the first synchrotron-based multi-element soft-X-ray STXM–NEXAFS spectromicroscopy experiment conducted at a submicrometer-scale on beamlines that can directly access the K- (C, N, Al and Si) and L- (Ca and Fe) edges of biogeochemically-relevant elements specifically targeting a physically entrapped particulate black C in undisturbed organomineral assemblage. This multi-element STXM–NEXAFS investigation enabled us to obtain element-specific high-resolution geobiological insight into the compositional chemistry and the various associative interactions and molecular-level linkages between black C, mineral matrix and non-black C organic matter present in the localized terminal submicron-C repository environment. The STXM–NEXAFS micrographs and spectra clearly demonstrated that the pyrogenic carbonaceous structure was dominated by quinones, unsaturated and aromatic hydrocarbons, phenols, ketones, carboxylic, alcohol, and hydroxylated- and ether-linked C functionalities. There was also evidence for the presence of pyridinic, pyridonic, pyrrolic, amine and nitril N functionalities. The biopolymer matrix in the organomineral complex was composed of amino acid, amino sugar, nucleic acid, and polysaccharide moieties from non-black C sources. These organic functionalities are known to exhibit negatively charged carboxylic, phenolic, enolic, thiolate and phosphate functionalities that are highly reactive towards black C and metal ions on account of their low isoelectric point and amphoteric nature. The metal-rich mineral matrix was composed of phyllosilicate clay minerals, Fe and Al hydroxypolycations, oxides, hydroxides and oxyhydroxide that can attract and bind organic biopolymers. Our results indicate interactive association between the pyrogenic structure, non-black C organic matter and the mineral oxide and oxyhydroxide communities in the organomineral assemblage. These intimate associations could occur through a “two-way” direct linkage of the black C, the mineral and non-black C organic matter or via a “three-way” indirect association where the non-black C organic matter could serve as a molecular cross-linking agent binding the black C with the mineral matter or vice versa where the inorganic oxides, hydroxides and polycations could act as a bridge to bind the black C with the non-black C organic matter. However, the staggering compositional complexity of black C and non-black C organic matter and the co-occurrence of mixed phyllosilicate and hydroxylated surface groups in the investigated organomineral interface seem to suggest that no single binding mechanism can be fully accountable for the apparent sequestration of organic C in the investigated terminal submicron-C repository environment. Rather the binding of black C with the mineral matrix and the non-black C organic matter in these micro- and nano-C repository environments seems to be the combined result of physical entrapment in terminal biotic exclusion zone through the action of metal oxides and organic matter induced microaggregation and the direct and indirect molecular-level associations ranging from ligand exchange, polyvalent cation bridging to weak hydrophobic interactions including van der Waals and H-bonding. Overall our results show significant progress towards directly identifying micro- and nano-environments of C sequestration and examining at submicron-level the compositional chemistry and interactions of black C, mineral and non-black C organic matter in these submicron-repository environments using STXM–NEXAFS spectromicroscopy. However, they also highlighted the need for additional investigations where nanoparticles separated only by atomically-thin wall being the designated basic system of interest to isolate and understand individual nano- and atomic-level biogeochemical binding mechanisms responsible for C sequestration in mineral soils.

Acknowledgments

This study was supported by grants from the Agriculture and Food Research Initiative Competitive Grant of the National Institute of Food and Agriculture (NIFA) (2008-35107-04511) and the Geobiology and Low-Temperature Geochemistry Program of the National Science Foundation (NSF) (EAR-0819689). The opinions and findings expressed in this material are those of the authors and do not reflect the views of NIFA or NSF. The C K-edge NEXAFS was recorded at X1A1 beamline of the National Synchrotron Light Source (NSLS). The N, Al, Si K-edge, and Ca and Fe L-edge NEXAFS were performed at SM 10ID-1 beamline of the Canadian Light Source (CLS).

References

Accardi-Dey A, Gschwend PM. Assessing the combined roles of natural organic matter and black carbon as sorbents in sediments. Environ Sci Technol 2002;36:21–9.
Achard FK. Chemische Untersuchung des Torfs. Crell's Chem Ann 1786;2:391–403.
Ade H, Urquhart SG. NEXAFS spectroscopy and microscopy of natural and synthetic polymers. In: Sham TK, editor. Chemical applications of synchrotron radiation. New Jersey: World Scientific Pub.; 2002. p. 285–355.
Baldock JA, Skjemstad JO. Role of the soil matrix and minerals in protecting natural organic materials against biological attack. Org Geochem 2000;31:697–710.
Benner R, Kaiser K. Abundance of amino sugars and peptidoglycan in marine particulate and dissolved organic matter. Limnol Oceanogr 2003;48:118–28.
Benzerara K, Yoon TH, Tyliszczak T, Constantz B, Spormann AM, Brown G. Scanning transmission X-ray microscopy study of microbial calcification. Geobiology 2004;2:249–59.
Boese J, Osanna A, Jacobsen C, Kirz J. Carbon edge XANES spectroscopy of amino acids and peptides. J Electron Spectrosc Relat Phenom 1997;85:9-15.
Brandes JA, Lee C, Wakeham S, Peterson M, Jacobsen C, Wirick S, et al. Examining marine particulate organic matter at sub-micron scales using scanning transmission X-ray microscopy and carbon X-ray absorption near edge structure spectroscopy. Mar Chem 2004;92:107–21.
Braun A, Mun BS, Huggins FE, Huffman GP. Carbon speciation of diesel exhaust and urban particulate matter NIST standard reference materials with C(1s) NEXAFS spectroscopy. Environ Sci Technol 2007;41:173–8.
Brodowski S, John B, Flessa H, Amelung W. Aggregate-occluded black carbon in soil. Eur J Soil Sci 2006;57:539–46.
Buckley CJ. The measuring and mapping of calcium in mineralized tissues by absorption difference imaging. Rev Sci Instrum 1995;66:1318–21.
Chenu C. Extracellular polysaccharides: an interface between microorganisms and soil constituents. In: Huang PM, et al, editor. Environmental impact of soil component interactions. Natural and anthropogenic organics. Florida: Lewis; 1995. p. 217–33.
Chenu C, Stotzky G. Interactions between microorganisms and soil particles: an overview. In: Huang PM, et al, editor. Interactions between soil particles and microorganisms. Impact on the terrestrial ecosystem. IUPAC series on analytical and physical chemistry of environmental systemsChichester: John and Sons; 2002. p. 1-40.
Cody GD, Ade H, Wirick S, Mitchell GD, Davis A. Determination of chemical–structural changes in vitrinite accompanying luminescence alteration using C-NEXAFS analysis. Org Geochem 1998;28:441–55.
Cody G, Ade H, Alexander C, Araki T, Butterworth A, Fleckenstein H, et al. Quantitative organic and light-element analysis of comet 81P/Wild 2 particles using C-, N-, and O-μ-XANES. Meteorit Planet Sci 2008;43:353–65.
Crocombette JP, Pollak M, Jollet F, Thromat N, Gautier-Soyer M. X-ray-absorption spectroscopy at the Fe $L_{2,3}$ threshold in iron oxides. Phys Rev B 1995;52:3143–50.
Doyle CS, Traina SJ, Ruppert H, Kendelewicz T, Rehr JJ, Brown GE. XANES studies at the Al K-edge of aluminum-rich surface phases in the soil environment. J Synchrotron Radiat 1999;6:621–3.
FAO-UNESCO. Soil map of the world, revised legend. Wageningen: ISRIC; 1997.
Fleet ME, Liu X. Calcium $L_{2,3}$-edge XANES of carbonates, carbonate apatite, and oldhamite (CaS). Am Mineral 2009;94:1235–41.
Francis JT, Hitchcock AP. Inner-shell spectroscopy of parabenzoquinone, hydroquinone, and phenol: distinguishing quinoid and benzenoid structures. J Phys Chem 1992;96:6598–610.
Gilbert B, Frazer BH, Naab F, Fournelle J, Valley JW, De Stasio G. X-ray absorption spectroscopy of silicates for in situ, sub-micrometer mineral identification. Am Mineral 2003;88:763–9.
Gillespie AW, Walley FL, Farrell RE, Regier TZ, Blyth RIR. Calibration method at the N K-edge using interstitial nitrogen gas in solid-state nitrogen-containing inorganic compounds. J Synchrotron Radiat 2008;15:532–4.
Glaser B, Haumaier L, Guggenberger G, Zech W. Black carbon in soils: the use of benzenecarboxylic acids as specific markers. Org Geochem 1998;29:811–9.
Haberstroh PR, Brandes JA, Gelinas Y, Dickens AF, Wirick S, Cody G. Chemical composition of the graphitic black carbon fraction in riverine and marine sediments at submicron scales using carbon X-ray spectromicroscopy. Geochim Cosmochim Acta 2006;70:1483–94.
Haumaier L, Zech W. Black carbon-possible source of highly aromatic components of soil humic acids. Org Geochem 1995;23:191–6.

Heymann K, Lehmann J, Solomon D, Schmidt MWI, Regier T. C 1s K-edge near-edge X-ray fine structure (NEXAFS) spectroscopy for characterizing the functional group chemistry of black carbon. Org Geochem 2011;42:1055–64.
Hitchcock AP. aXis2000 an interactive data language (IDL). http://unicorn.mcmaster.ca/aXis2000.html 2008.
Hitchcock AP, Ishii I. Carbon K-shell excitation-spectra of linear and branched alkanes. J Electron Spectrosc Relat Phenom 1987;42:11–26.
Hitchcock AP, Dynes JJ, Lawrence JR, Obst M, Swerhone GDW, Korber DR, et al. Soft X-ray spectromicroscopy of nickel sorption in a natural river biofilm. Geobiology 2009;7:432–53.
Hu YF, Xu RK, Dynes JJ, Blyth RIR, Yu G, Kozak LM, et al. Coordination nature of short-range ordered aluminum (oxy)hydroxides formed under the influence of tannic acid studied by X-ray absorption spectroscopy. Geochim Cosmochim Acta 2008;72:1959–69.
Huang PM. Soil mineral–organic matter–microorganism interactions: fundamentals and impacts. Adv Agron 2004;82:391–472.
Ildefonse P, Cabaret D, Sainctavit P, Calas G, Flank AM, Lagarde P. Aluminum X-ray absorption near edge structure in model compounds and Earth's surface minerals. Phys Chem Miner 1998;25:112–21.
Ishii I, Hitchcock AP. The oscillator strengths for C1s and O1s excitation of some saturated and unsaturated organic alcohols, acids, and esters. J Electron Spectrosc Relat Phenom 1988;46:55–84.
Jacobsen C, Wirick S, Flynn G, Zimba C. Soft X-ray spectroscopy from image sequences with sub-100 nm spatial resolution. J Microsc 2000;197:173–84.
Joseph SD, Camps-Arbestain M, Lin Y, Munroe P, Chia CH, Hook J, et al. An investigation into the reactions of biochar in soil. Aust J Soil Res 2010;48:501–15.
Kaznacheyev K, Osanna A, Jacobsen C, Plashkevych O, Vahtras O, Ågren H, et al. Inner-shell absorption spectroscopy of amino acids. J Chem Phys 2002;106:3153–68.
Kaznatcheev KV, Karunakaran C, Lanke UD, Urquhart SG, Obst M, Hitchcock AP. Soft X-ray spectromicroscopy beamline at the CLS: commissioning results. Nucl Inst Methods Phys Res A 2007;582:96–9.
Keiluweit M, Nico PS, Johnson MG, Kleber M. Dynamic molecular structure of plant biomass-derived black carbon (biochar). Environ Sci Technol 2010;44:1247–53.
Kinyangi J, Solomon D, Liang B, Lerotic M, Wirick S, Lehmann J. Nanoscale biogeocomplexity of the organo-mineral assemblage in soil: application of STXM microscopy and C 1s-NEXAFS spectroscopy. Soil Sci Soc Am J 2006;70:1708–18.
Kleber M, Sollins P, Sutton R. A conceptual model of organo-mineral interactions in soils: self-assembly of organic molecular fragments into zonal structures on mineral surfaces. Biogeochemistry 2007;85:9-24.
Kolczewski C, Puttner R, Martins M, Schlachter AS. Spectroscopic analysis of small organic molecules: a comprehensive near-edge X-ray absorption fine-structure study of C6-ring-containing molecules. J Chem Phys 2006;124:034302.
Kruse J, Eckhardt K-U, Regier T, Leinweber P. TG–FTIR, LC/MS, XANES and Py-FIMS to disclose the thermal decomposition pathways and aromatic N formation during dipeptide pyrolysis in a soil matrix. J Anal Appl Pyrolysis 2011;90:164–73.
Ledin M, Krantz-Rulcker C, Allard B. Microorganisms as metal sorbents: comparison with other soil constituents in multi-compartment systems. Soil Biol Biochem 1999;31:1639–48.
Lehmann J, Solomon D. Organic carbon chemistry in soils observed by synchrotron-based spectroscopy. In: Singh B, Gräfe M, editors. Synchrotron-based techniques in soils and sediment. Amsterdam: Elsevier; 2010. p. 289–312.
Lehmann J, Liang B, Solomon D, Lerotic M, Luizão F, Kinyangi F, et al. Near-edge X-ray absorption fine structure (NEXAFS) spectroscopy for mapping nano-scale distribution of organic carbon forms in soil: application to black carbon particles. Global Biogeochem Cycles 2005;19:GB1013.
Lehmann J, Solomon D, Kinyangi J, Dathe L, Wirick S, Jacobson C. Spatial complexity of soil organic matter forms at nanometer scales. Nat Geosci 2008;1:238–42.
Leinweber P, Kruse J, Walley FL, Gillespie A, Eckhardt KU, Blyth RIR, et al. Nitrogen K-edge XANES — an overview of reference compounds used to identify 'unknown' organic nitrogen in environmental samples. J Synchrotron Radiat 2007;14:500–11.
Lerotic M, Jacobsen C, Schäfer T, Vogt S. Cluster analysis of soft X-ray spectromicroscopy data. Ultramicroscopy 2004;100:35–57.
Li D, Bancroft GM, Fleet ME, Feng XH. Silicon K-edge XANES spectra of silicate minerals. Phys Chem Miner 1995a;22:115–22.
Li D, Bancroft GM, Fleet ME, Feng XH, Pan Y. Al K-edge XANES spectra of aluminosilicate minerals. Am Mineral 1995b;80:432–40.
Liang B, Lehmann J, Solomon D, Kinyangi J, Grossman J, O'Neill B, et al. Black carbon increases cation exchange capacity in soils. Soil Sci Soc Am J 2006;70:1719–30.
Loganathan VA, Feng Y, Sheng GD, Clement TP. Crop-residue-derived char influences sorption, desorption and bioavailability of atrazine in soils. Soil Sci Soc Am J 2009;73:967–74.
Lützow VM, Kögel-Knabner I, Ekschmitt K, Matzner E, Guggenberger G, Marschner B, et al. Stabilization of organic matter in temperate soils: mechanisms and their relevance under different soil conditions — a review. Eur J Soil Sci 2006;57:426–45.
Mahamid J, Aichmayer B, Shimoni E, Ziblat R, Li C, Siegel S, et al. Mapping amorphous calcium phosphate transformation into crystalline mineral from the cell to the bone in zebrafish fin rays. Proc Natl Acad Sci 2010;107:6316–21.
Miot J, Benzerara K, Morin G, Kappler A, Bernard S, Obst M, et al. Iron biomineralization by anaerobic neutrophilic iron-oxidizing bacteria. Geochim Cosmochim Acta 2009;73:696–711.
Mitra-Kirtley S, Mullins OC, Branthaver JF, Cramer SP. Nitrogen chemistry of kerogens and bitumens from X-ray absorption near-edge structure spectroscopy. Energy Fuel 1993a;7:1128–34.
Mitra-Kirtley S, Mullins OC, van Elp J, George SJ, Chen J, Cramer SP. Determination of the nitrogen chemical structures in petroleum asphaltenes using XANES spectroscopy. J Am Chem Soc 1993b;115:252–8.
Mitra-Kirtley S, Mullins OC, van Elp J, Cramer SP. Nitrogen XANES studies of Argonne coals. ACS Div Fuel Chem 1994;39:820–4.
Mullins OC, Mitra-Kirtley S, van Elp J, Cramer SP. Molecular structure of nitrogen in coal from XANES spectroscopy. Appl Spectrosc 1993;47:1268–75.
Naftel SJ, Sham TK, Yiu YM, Yates BW. Calcium L-edge XANES study of some calcium compounds. J Synchrotron Radiat 2001;8:255–7.
Obst M, Dynes JJ, Lawrence JR, Swerhone GDW, Karunakaran C, Kaznacheyev K, et al. Precipitation of amorphous $CaCO_3$ (aragonite) controlled by cyanobacteria: a multi-technique study of the influence of EPS on the nucleation process. Geochim Cosmochim Acta 2009;73:4180–98.
Pels JR, Kapteijn F, Moulijn JA, Zhu Q, Thomas KM. Evolution of nitrogen functionalities in carbonaceous materials during pyrolysis. Carbon 1995;11:1641–53.
Pignatello JJ, Kwon S, Lu Y. Effect of natural organic substances on the surface and adsorptive properties of environmental black carbon (char): attenuation of surface activity by humic and fulvic acids. Environ Sci Technol 2006;40:7757–63.
Politi Y, Metzler RA, Abrecht M, Gilbert B, Wilt FH, Sagi I, et al. Transformation mechanism of amorphous calcium carbonate into calcite in the sea urchin larval spicule. Proc Natl Acad Sci 2008;45:17362–6.
Preston CM, Schmidt MWI. Black (pyrogenic) carbon: a synthesis of current knowledge and uncertainties with special consideration of boreal regions. Biogeoscience 2006;3:397–420.
Samuel NT, Lee CY, Gamble LJ, Fischer DA, Castner DG. NEXAFS characterization of DNA components and molecular-orientation of surface bound DNA oligomers. J Electron Spectrosc Relat Phenom 2006;152:134–42.
Sato S, Solomon D, Hyland C, Ketterings QM, Lehmann J. Phosphorus speciation in manure and manure-amended soils using XANES spectroscopy. Environ Sci Technol 2005;39:7485–91.
Sato S, Neves EG, Solomon D, Liang B, Lehmann J. Biogenic calcium phosphate transformation in soils over millennium time scales. J Soils Sediment 2009;9:194–205.
Schäfer T, Buckau G, Artinger R, Kim JI, Geyer S, Wolf M, et al. Origin and mobility of fulvic acids in the Gorleben aquifer system: implications from isotopic data and carbon/sulfur XANES. Org Geochem 2005;36:567–82.
Schloesing T. Etudes sur la terre vegetale. C R Hebd Seances Acad Sci 1902;135:601–5.
Schulten H-R, Schnitzer M. The chemistry of soil organic nitrogen: a review. Biol Fertil Soils 1998;26:1-15.
Shafizadeh F, Sekiguchi Y. Development of aromaticity in cellulosic chars. Carbon 1983;21:511–6.
Sham TK, Yang BX, Kirz J, Tse JS. K-edge near-edge X-ray absorption fine structure of oxygen- and carbon-containing molecules in the gas phase. Phys Rev A 1989;40:652–69.
Shaw SA, Peak D, Hendry MJ. Investigation of acidic dissolution of mixed clays between pH 1.0 and 3.0 using Si and Al X-ray absorption near edge structure. Geochim Cosmochim Acta 2009;73:4151–65.
Skjemstad JO, Bushby HVA, Hansen RW. Extractable Fe in the surface horizons of a range of soils from Queensland. Aust J Soil Res 1989;28:259–66.
Sollins P, Homann P, Caldwell BA. Stabilisation and destabilisation of soil organic matter: mechanisms and controls. Geoderma 1996;74:65-105.
Solomon D, Lehmann J, Kinyangi J, Liang B, Schäfer T. Carbon K-edge NEXAFS and FTIR-ATR spectroscopic investigation of organic carbon speciation in soils. Soil Sci Soc Am J 2005;69:107–19.
Solomon D, Lehmann J, Thies J, Schäfer T, Liang B, Kinyangi J, et al. Molecular signature and sources of biochemical recalcitrance of organic C in Amazonian Dark Earths. Geochim Cosmochim Acta 2007;71:2285–98.
Solomon D, Lehmann J, Kinyangi J, Liang B, Hanley K, Heymann K, et al. Carbon (1s) NEXAFS spectroscopy of biogeochemically relevant organic reference compounds. Soil Sci Soc Am J 2009;73:1817–30.
Sposito G. The chemistry of soils. New York: Oxford University Press; 2008.
Stöhr J, Samant MG, Lüning J, Callegari AC, Chaudhari P, Doyle JP, et al. Liquid crystal alignment on carbonaceous surfaces with orientational order. Science 2001;292:2299–302.
Tarnocai C, Canadell JG, Schuur EAG, Kuhry P, Mazhitova G, Zimov S. Soil organic carbon pools in the northern circumpolar permafrost region. Glob Biogeochem Cycles 2009;19:GB2023.
Trumbore S. Radiocarbon and soil carbon dynamics. Annu Rev Earth Planet Sci 2009;37:47–66.
Urrutia MM, Beveridge TJ. Formation of fine-grained metal and silicate precipitates on a bacterial surface (*Bacillus subtilis*). Chem Geol 1994;116:261–80.
Vairavamurthy A, Wang S. Organic nitrogen in geomacromolecules: insights on speciation and transformation with K-edge XANES spectroscopy. Environ Sci Technol 2002;36:3050–6.
van Aken PA, Liebscher B. Quantification of ferrous/ferric ratios in minerals: new evaluation schemes of Fe $L_{2,3}$ electron energy-loss near-edge spectra. Phys Chem Miner 2002;29:188–200.
Van derlaan G, Kirkman IW. The 2p absorption spectra of 3d transition metal compounds in tetrahedral and octahedral symmetry. J Phys Condens Matter 1992;4:4189–204.
Vermeer AWP, van Riemsdijk WH, Koopal LK. Adsorption of humic acids to mineral particles. 1. Specific and electrostatic interactions. Langmuir 1998;14:2810–9.
Violante A, Krishnamurti GSR, Huang PM. Impact of organic substances on the formation and transformation of metal oxides in soil environments. In: Huang PM, Bollag J-M, Senesi N, editors. Impact on the ecosystem, IUPAC series on analytical and physical chemistry of environmental systemsChichester: John and Sons; 2002. p. 133–88.
Wada K. Role of aluminium and iron in the accumulation of organic matter in soils with variable charge. In: Huang PM, Berthelin J, Bollag J-M, McGill WB, Page AL, editors. Environmental impact of soil component interactions. Boca Raton: CRC Lewis; 1995. p. 47–58.
Wan J, Tyliszczak T, Tokunaga TK. Organic carbon distribution, speciation, and elemental correlations within soil microaggregates: applications of STXM and NEXAFS spectroscopy. Geochim Cosmochim Acta 2007;71:5439–49.

Wirick S, Flynn GJ, Keller LP, Nakamura-Messenger K, Peltzer C, Jacobsen C, et al. Organic matter from comet 81P/Wild 2, IDPs, and carbonaceous meteorites; similarities and differences. Meteorit Planet Sci 2009;44:1611–26.
Yoon TH, Johnson SB, Benzerara K, Doyle CS, Tyliszczak T, Shuh DK, et al. In-situ characterization of aluminum coating mineral–microorganism aqueous suspensions using scanning transmission X-ray microscopy. Langmuir 2004;20:10361–6.
Yoon TH, Benzerara K, Ahn S, Luthy RG, Tyliszczak T, Brown GE. Nanometer-scale chemical heterogeneities of black carbon materials and their impacts on PCB sorption properties: soft X-ray spectromicroscopy study. Environ Sci Technol 2006;40:5923–9.
Zhu Q, Money SL, Russell AE, Thomas KM. Determination of the fate of nitrogen functionality in carbonaceous materials during pyrolysis and combustion using X-ray absorption near edge structure spectroscopy. Langmuir 1997;13:2149–57.
Zhuang J, Yu G. Effects of surface coatings on electrochemical properties and contaminant sorption of clay minerals. Chemosphere 2002;49:619–28.
Zubavichus Y, Shaporenko A, Grunze M, Zharnikov M. Innershell absorption spectroscopy of amino acids at all relevant absorption edges. J Phys Chem A 2005;109:6998–7000.